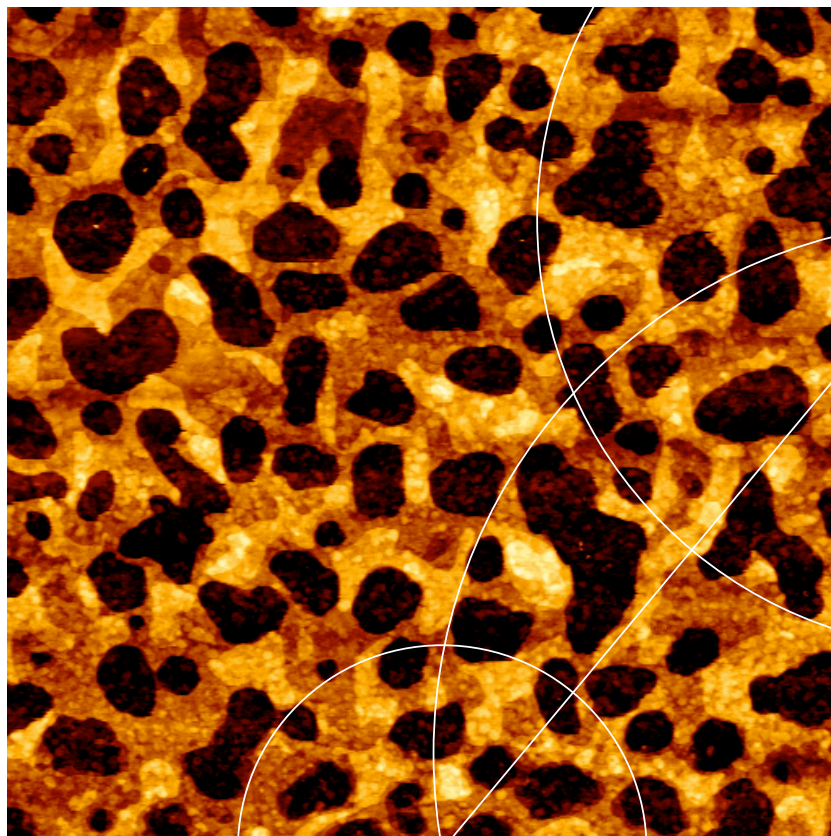




## Master's thesis

Stanislav Landa

# Influence of voltage on phase behaviour of membranes



Academic advisor: Thomas Heimburg

Submitted: 31/07/13



## Abstract

The Soliton model explains nerve signal propagation in the membranes of axons. According to the model this propagation locally pushes the membrane into its phase transition. Mechanical, electrical and chemical stimuli have been claimed to move the phase transition and melting temperature of the membrane. The aim of this thesis is to investigate the effect of an external voltage on the phase transition on supported lipid membranes.

As a model system a mixture of DPPC and DLPC in the ratio 65% to 35% in aqueous solution is deposited on three different solid supports: mica, indium tin oxide covered glass and graphene covered glass. Atomic force microscopy is used to investigate the change in lipid membrane thickness when voltage is applied. The temperature associated with the phase transition of the lipid mixture was determined using differential scanning calorimetry. The experiments have been performed accordingly at 23°C.

Thickness decrease of the membrane is observed for voltages under 1 V on both ITO and graphene supports and attributed to a transition from gel to fluid state. Higher voltages induce a thickness increase, which is attributed to dissociation of membrane layers from each other.

## Resumé

Solitonmodellen forklarer udbredning af nervesignaler i aksoners membraner. Ifølge modellen skubber denne udbredelse lokalt membranen ind i dens faseovergang. Mekaniske, elektriske og kemiske stimuli hævdes at kunne flytte membranens faseovergang og smeltetemperatur. Målet med denne opgave er at undersøge effekten af en ekstern spændingsforskel på faseovergangen af supported lipid membranes.

Som modelsystem deponeres en vandig opløsning af DPPC og DLPC i blandingsforholdet 65% til 35% på tre forskellige faste underlag: mica, glas dækket med indiumtinoxid og med grafen. Atomart kraftmikroskopi bruges til at undersøge ændringen i lipidmembranes højde, når spænding påføres. Temperaturafhængigheden af faseovergangen for lipidblandingen blev bestemt ved differential skanningskalorimetri. Eksperimenterne blev passende udført ved 23°C.

Der ses, at membrantykkelsen falder for spændingsforskelle på under 1 V, både på ITO- og grafensupport, og det tilskrives en overgang fra gel til flydende tilstand. Højere spændingsforskelle fremkalder en forøgelse af tykkelsen, som tilskrives en dissociation mellem flere membranlag.

## Acknowledgements

I would like to thank:

- Thomas Heimbürg for giving me the opportunity to write this thesis. It has been an interesting topic and a good learning experience.
- Alfredo González-Pérez for being a great colleague in the lab, providing me with ideas and insight into my experiments, and for proofreading my thesis.
- Lars Dalskov Mosgaard for discussions on the topic and for proofreading of the thesis.
- Rolf Justesen Pedersen for introducing me to use the AFM equipment.
- Marie Domange Jordö for introducing me to the lab procedures and sample preparation.
- Søren Blok Madsen for introducing me to the DSC equipment.
- Vedran Šekara for proofreading the thesis.
- All the people in the K-building for being such a lovely bunch, with whom I could drink coffee and play foosball in the breaks.
- And of course my parents and my brother for supporting me during my studies and my entire life.

Without you all this would not have been possible.

## Abbreviations

DPPC – 1,2-Dipalmitoyl-sn-phosphatidylcholine

DMPC – 1,2-Dimyristoyl-sn-phosphatidylcholine

DLPC – 1,2-Dilauroyl-sn-phosphatidylcholine

AFM – Atomic force microscope(y)

DSC – Differential scanning calorimetry

ITO – Indium tin oxide



# Contents

<b>1</b>	<b>Introduction</b>	<b>1</b>
<b>2</b>	<b>Membranes</b>	<b>5</b>
2.1	Lipids . . . . .	6
2.1.1	Phospholipids . . . . .	6
2.1.2	Self-assembly . . . . .	7
2.2	Thermodynamics . . . . .	8
2.2.1	Lipid phases . . . . .	8
2.2.2	Phase transition . . . . .	10
2.2.3	Proteins . . . . .	11
<b>3</b>	<b>Nerves</b>	<b>13</b>
3.1	Structure . . . . .	13
3.2	Hodgkin-Huxley Model . . . . .	14
3.2.1	Shortcomings of the Hodgkin-Huxley model . . . . .	17
3.3	The Soliton Model . . . . .	18
<b>4</b>	<b>Materials and Methods</b>	<b>21</b>
4.1	Materials . . . . .	21
4.1.1	Chemicals . . . . .	21
4.1.2	Equipment . . . . .	22
4.2	Differential scanning calorimetry . . . . .	22
4.2.1	The basics . . . . .	23
4.2.2	Operation . . . . .	23
4.3	Atomic Force Microscopy . . . . .	24
4.3.1	The microscope . . . . .	25
4.3.2	Operation . . . . .	26
4.3.3	Sample preparation . . . . .	29
4.3.4	Cleaning procedure . . . . .	30

<b>5</b>	<b>Results and Discussion</b>	<b>33</b>
5.1	Calorimetry . . . . .	33
5.2	Atomic force microscopy . . . . .	35
5.2.1	Experiments on mica in air . . . . .	35
5.2.2	Experiments on mica in water . . . . .	38
5.2.3	Experiments on ITO in water . . . . .	39
5.2.4	Experiments on ITO using TFE as solvent . . . . .	40
5.2.5	Experiments on ITO with an external electric field . . . . .	42
5.2.6	Experiments on graphene with an external electric field . . . . .	45
<b>6</b>	<b>Discussion</b>	<b>49</b>
<b>7</b>	<b>Conclusion</b>	<b>51</b>
<b>A</b>	<b>Stock solution preparation</b>	<b>53</b>
<b>B</b>	<b>Further images</b>	<b>55</b>

# Chapter 1

## Introduction

Since before the dawn of civilisation Man has observed both the living and inanimate nature of the world, tried to understand it and eventually bend it to serve his will. Prehistoric times produced primitive tools and weapons, agriculture, early music and art forms and the gradual mastering of new materials. The birth of civilisation and complex language eventually created scientific disciplines such as mathematics, philosophy and physics, posing the mind-boggling question puzzling us until this day - *Who are we?*

A part of this question relates to our physical nature. The separation of disease from divinity and superstition is accredited to the father of Western medicine, Hippocrates of Kos (BCE c.460-c.370), in essence creating the field of medicine that attempted to diagnose and cure illness. In his dissections and experiments on pigs and primates Aelius Galenus (CE 129-c.200) showed the functions of motor nerves in muscle and limb functions simultaneously initiating an experimental approach to physiology. Luigi Galvani's (1737-1798) experiments with frogs lead in 1771 to his discovery of electrical charge affecting and animating the nervous system, which he coined *animal electricity* and believed originated from within the organism. This was later disproved by Alessandro Volta (1745-1827), who proposed that the frog's limbs merely served as a conductor of electricity. It has since been shown that cells maintain an electric gradient across their membrane, which plays a crucial role in their functioning.

A biological cell is a compartment containing genetic information, a physical structure, necessary chemical ingredients and functionality to maintain its life. It is separated from the world by a complex membrane, consisting of lipids and proteins that enable it to respond to and function in its surroundings. Many of a cell's vital processes involve the membrane, such as maintaining chemical and electrical gradients across, transporting nutrients and waste, sensory functions. Life on Earth began with single-cell organ-

isms c. 4.5-3.5  $Ga$ <sup>1</sup> ago, whose descendants still play a critical role in the biosphere, but about 1.7  $Ga$  ago multicellular life emerged, and cells were required to specialise. In higher organisms eventually an important type of cells emerged - the nerve cell, which acted as a long-distance signal carrier. The propagation of these signals has also been attributed to the nerve cells' membranes.

In 1952 Hodgkin and Huxley proposed the now widely accepted theory of nerve signal propagation [1]. Their model is based on time- and voltage-dependent transmembrane proteins called ion channels, which by selective conductance of ions alter the voltage across the membrane. In turn, this change initiates a recursive effect, which produces a traveling voltage pulse along the nerve. The nerve cell itself can be schematically visualised as a set of Kirchhoff's circuits, the membrane acting as an imperfect capacitor with leak currents and the ion channels – as resistors (Fig. 3.3). This model assumes nerve propagation to be a dissipative phenomenon based on equilibration of ionic currents and the resistors being the heat producing elements. However, experiments [2] have shown that nerve pulses are adiabatic in nature, releasing heat initially, but reabsorbing it upon relaxation.

Addressing this discrepancy Heimburg and Jackson have recently proposed a new thermodynamic model [2] treating nerve signals as localised density pulses, *solitons*, in nerve membranes. By exhibiting the adiabatic behavior during propagation of nerve signals, this Soliton model also explains other physical changes that have previously been observed and linked to signal propagation: thickness change of the membrane and length change of the nerve. It also makes correct predictions about signal velocity in myelinated nerves and provides better insight in the function of general anaesthetics.

The biological membrane is the medium of these events, and its composition dictates its physical properties and the changes to these that can occur. By far the most abundant component of the membrane is a class of small molecules called *lipids*, which serve as a sheet into which other, larger units such as proteins are embedded. This combined mass of molecules can exist in at least two phases, an ordered and disordered, and in the phase transition between them the properties and behaviour of a membrane can change dramatically. Typically the phase transition lies close to the physiological temperature of a particular organism, the composition will even change according to external living conditions, and it is thus thought likely that the phase transition plays a pivotal role for physiology. Different stimuli have been shown to shift the state of the membrane, including temperature, pressure, electric and chemical gradients.

---

<sup>1</sup> $Ga$  - gigaannum,  $10^9$  years.

The soliton model claims nerve signal transmission to push the membrane through its phase transition locally. It is therefore of importance to find out how an external electric field can affect the phase transition and thereby nerve signal propagation. The goal of this thesis is to explore how the application of an external voltage over a membrane affects its physical properties. In this thesis the change in membrane thickness will be the measure that determines the shift through the phase transition. Atomic force microscopy will serve as the method for detecting this change.

At first the reader will be introduced to the underlying theoretical knowledge in **Membranes** (chapter 2) and **Nerves** (chapter 3). Chapter 4 will summarise the chemicals used, instrumentation, and explain the experimental procedures used during this project. Chapter 5 will present the data obtained as well as its analysis. Finally, the **Discussion** and **Conclusion** will summarise this master's thesis and its results into a broader perspective.



# Chapter 2

## Membranes

By the end of the 19th century several botanical studies had shown that the inside of the cell was separated from its surroundings by an osmotic barrier. Pfeffer was the first to propose the *plasma membrane* in his work in 1877 [3], and Overton postulated it to be an oily substance in 1895. In 1925 Gorter and Grendel experimentally showed [4] that the oily plasma membrane was actually a film just two molecules thick by comparing the surface area of red blood cells' membranes from a microscope image to measurements with a Langmuir trough. Their simple theory said that the cell membrane must consist of two lipid monolayers with their non-polar tails pointing towards each other and the polar headgroups outwards, which became the basis for later membrane models. Ten years later Danielli and Davson [5] extended this model by noting the large amount of protein present in the membrane, however they falsely assumed that proteins made up separate layers on each side of the membrane.



Figure 2.1: Patches of membrane models for illustration. *Left*, the Fluid Mosaic model; *right*, the Mattress model [6].

Due to advance in technology Singer and Nicolson could in 1972 propose

an updated picture of the cell membrane, the *Fluid Mosaic model* (Fig. 2.1, left) [7], which embedded proteins in a two-dimensional homogeneous lipid membrane and gave them freedom of diffusion inside it. In 1984 Mouritsen and Bloom [8] upgraded the model by accounting for asymmetry of lipid composition between the two monolayers as well as an inhomogeneous lateral distribution of lipids due to physical characteristics and lipid-lipid and lipid-protein interactions. Their *Mattress model* (Fig. 2.1, right) describes the bilayer as a very flexible medium arranging itself to energetically favourable configurations depending on hydrophobic matching.

The following parts of this chapter will cover the building blocks of the membrane and the physical laws that govern their behavior.

## 2.1 Lipids

Lipids are part of a wide variety of molecules called amphiphiles. These molecules are characterised by the presence of two distinctive affinities: one part of the molecule is hydrophobic, the other – hydrophilic. Their ability to self-assemble comes from these properties.

The simplest constructs are the fatty acids of the form  $\text{RCOOH}$ , with R being a hydrocarbon chain. They are, however, typically not found as free molecules, but are present as parts of other more complex lipids, such as the phospholipids or triglycerides. These two types use a glycerol backbone with, respectively, either two or three fatty acids attached; instead of a third carboxylic acid phospholipids have a polar headgroup. Sphingolipids are more complex, using only one fatty acid and additional headgroups. The sterols, part of the steroid group, use a hydroxylated backbone of four cycloalkane rings. Of these families the phospholipids are by far the most abundant in biological membranes [9].

### 2.1.1 Phospholipids

As mentioned above, the phospholipids have a glycerol backbone. The hydroxides in the first and second positions are substituted by fatty acids with even-length carbon chains with a typical length of 16 or 18, but can in general be between 12 and 24 molecules long [10]. The chains can be saturated or unsaturated. The glycerol's third hydroxide is replaced by a phosphate group, to which in turn is attached a polar headgroup. This structure produces an amphiphilic molecule with two hydrophobic tails and a hydrophilic headgroup (Fig. 2.2).

The headgroup of a phospholipid can be derived from one of the following

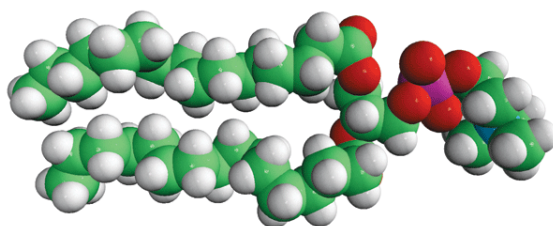


Figure 2.2: An example of a phospholipid, DPPC, with two hydrocarbon chains connected with a glycerol to a phosphocholine group. The pink atom is phosphorus and blue is nitrogen [11].

molecules: choline, ethanolamine, serine or glycerol. Since there is a negative charge on the phosphorus atom, choline and ethanolamine headgroups show zwitterionic properties due to the positively charged nitrogen atom at their extremity. In the case of serine and glycerol the headgroup is negatively charged. Typically, 10-20% of lipids in a membrane are charged, but this number can rise up to 40% in the membrane of mitochondria [10].

The IUPAC<sup>1</sup> nomenclature is simple for phospholipids, mentioning firstly the two fatty acids and then the headgroup. The following table mentions the most common components:

<b>Saturated acids:</b>			<b>Headgroups:</b>	
Lauric	(12C)	$\text{CH}_3(\text{CH}_2)_{10}\text{COOH}$	Choline	$(\text{CH}_3)_3\text{N}^+\text{CH}_2\text{CH}_2\text{OH}$
Myristic	(14C)	$\text{CH}_3(\text{CH}_2)_{12}\text{COOH}$	Ethanolamine	$\text{H}_2\text{NCH}_2\text{CH}_2\text{OH}$
Palmitic	(16C)	$\text{CH}_3(\text{CH}_2)_{14}\text{COOH}$	Serine	$\text{HOOCCH}(\text{NH}_2)\text{CH}_2\text{OH}$
Stearic	(18C)	$\text{CH}_3(\text{CH}_2)_{16}\text{COOH}$	Glycerol	$(\text{CH}_3\text{OH})_2\text{CH}_2\text{OH}$

An example could be **palmitoyl-lauroyl-sn-phosphatidylcholine**, or PLPC for short.

### 2.1.2 Self-assembly

Due to the amphipilic nature of lipids, they can self-assemble [12] into a variety of structures. Because of the molecules' polarity, in a polar medium such as water the headgroups will turn outwards, while they will turn inwards in an oily substrate. For single-tailed lipids the simplest self-assembled structure is a micelle that can aggregate in to a number of different morphologies

<sup>1</sup>The International Union of Pure and Applied Chemistry (UIPAC) is an international, scientific, non-governmental body. Among its functions are the nomenclature of chemical substances, standardisation of atom wights and physical constants.

(Fig. 2.3). Phospholipids assemble into more complex membrane structures called vesicles (Fig. 2.3). This is in essence the simplest form of biological cell and is therefore a perfect model system when working with membranes. Although concentration plays an important role for the lipids' aggregation, other parameters, such as pH, temperature, pressure and salinity will affect spontaneous assembly as well.

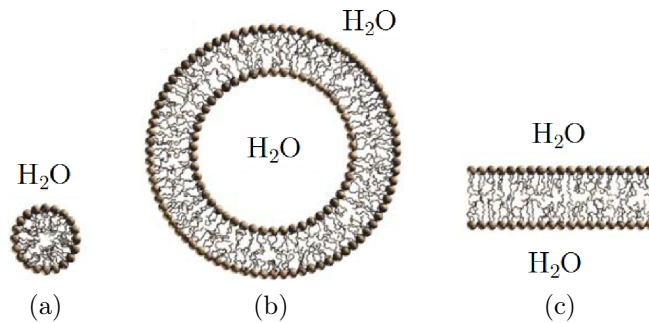


Figure 2.3: Different ways lipids can assemble. From left to right: a micelle, a vesicle and a bilayer [6].

## 2.2 Thermodynamics

As the model system has now been introduced, we move on to its more detailed physical description.

### 2.2.1 Lipid phases

Similar to other materials the membrane can be found in several thermodynamic states, and while for everyday substances solid, liquid and gaseous states are typically observed, the transitions through the membrane's four phases are explained further below. The phases are dependent on concentration and temperature, because the carbon-carbon bonds can twist into three different positions. Figure 2.4 depicts the energy minima the bonds can be found in, the lowest being the *trans*-conformation, when the two carbon atoms are farthest apart from each other. An all-*trans* lipid tail will take the form of a zig-zag and have the longest physical extension. The other two positions are the *gauche*<sup>±</sup>, the C atom rotated 120° either way. The *gauche* state is naturally not static, and a C-C bond can "relax" as the internal energy transfers to another bond in the tail. This results in a *melted*

molecule, twisting even more with additional temperature and changing its physical conformation as well as occupied volume. The description of the membrane phases now follows:

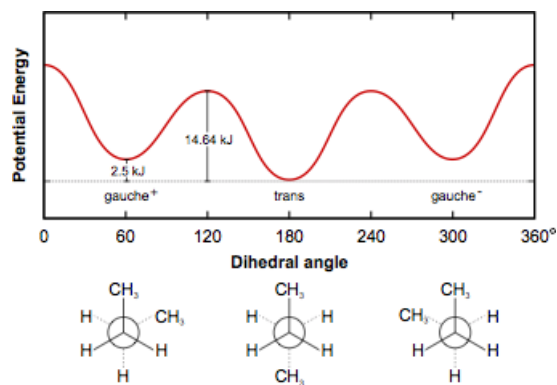


Figure 2.4: Energy levels for *trans* and *gauche*<sup>±</sup> C-C bond configuration [6].

- $L_c$  – The crystalline lipid phase occurs at lower temperatures. The membrane is ordered in three dimensions, laterally in a triangular lattice, and with all C-C bonds in the *trans* conformation.
- $L_{\beta'}$  – This is the solid ordered phase, also called the gel phase. Lipids are found in an ordered membrane. Lipid tails are mostly in an all-*trans* conformation and some headgroups are tilted with respect to the normal of the plane.
- $P_{\beta'}$  – The ripple phase, can be observed before the membrane's main phase transition. It can be very elusive as it appears in a very narrow temperature range. The ripples are a periodic one-dimensional formation and consist of liquid ( $L_\alpha$ ) and gel-like ( $L_{\beta'}$ ) domains. The ripple phase only occurs in some systems and is very fragile.
- $L_\alpha$  – The fluid, or liquid-disordered, phase is found right after the main phase transition. The C-C chain order is gone due to high internal energy in the molecules; lattice structure is also lost and the lipids move freely around.

Further on, this thesis will consider the  $L_{\beta'}$  and  $L_\alpha$  phases and the main transition between them, while the ripple phase will be disregarded. This is an acceptable simplification, since the ripple phase plays an almost non-existing role in biomembranes.

### 2.2.2 Phase transition

Just as ice melts to water, so does a membrane go from its solid state to liquid when heated. As described above, in the phase transition the lipid tails become disordered due to increased entropy in the system, and this gives rise to a change in the physical susceptibilities. The transition is a cooperative behavior, which occurs in a narrow temperature window. A system is typically lead through the phase transition by heating, experimentally this can be done with differential scanning calorimetry (DSC), which records heat uptake upon temperature increase – this will further be mentioned in section 4.2. In the ideal case the phase transition is a process of the system absorbing energy whilst remaining at constant temperature. Cooperativity during the melting process is a factor that aids this; lipids favour melting in clusters. Multilamellar vesicles can show a very sharp peak in their melting profile, less than  $0.1^\circ$  [10], but for natural biological membranes cooperativity must also be considered, though their transition window can span up to  $30^\circ$ . Figure 2.5 shows a melting profile for E. Coli, while section 5.1 shows several melting profiles for lipids.

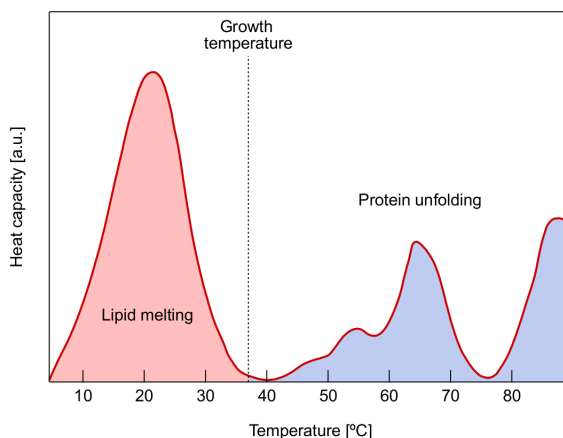


Figure 2.5: Heat capacity profile for E. Coli. [13]

The cooperative melting behavior is very well depicted with fluorescent microscopy. In figure 2.6, where the membrane is in transition, differently shaded domains correspond to aggregated lipid clusters in either the solid or liquid phases.

In biological membranes phase transitions have been observed to occur just below physiological growth temperatures, and organisms have shown to adapt their membrane composition in order to conserve this relation [10].

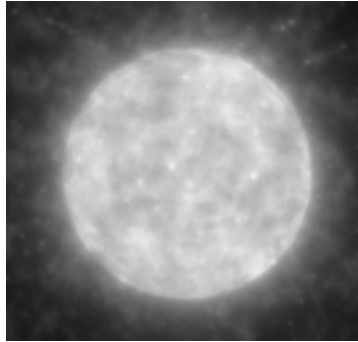


Figure 2.6: Image of a vesicle obtained with fluorescent microscopy.

This coupling indicates the phase transition to be crucial for organisms' functioning and has sparked extensive research in this field

Another important point to notice is the effect of proteins on the membrane and its phase transition. Biological membranes can contain up to 50% protein by mass, and they can alter the temperature window and location of the phase transition. In turn the lipid phase behaviour can affect the functionality of membrane proteins. Protein presence can be detected in calorimetric scans.

### 2.2.3 Proteins

When discussing biological membranes it is impossible to overlook proteins and their interaction with lipids. Proteins are synthesised in the cytoplasm of the cell by ribosomes. After the assembly of amino acid chains the proteins fold into a final 3-dimensional structure and travel to the destination, where their functionality lies. In case of membrane proteins this is either in the main cell membrane or one belonging to the organelles, such as the nucleus or the lysosomes.

Membrane proteins can be divided into two main groups based on their physical structure and functional location with regards to the membrane. Both types associate themselves with the membrane: peripheral proteins interact with one side only, while integral, or transmembrane, proteins connect functions from both sides. The tertiary structure of a protein places some hydrophobic amino acids on its periphery, which due to the hydrophobic effect and entropy results in its incorporation into the membrane's interior. However, since both proteins and lipids vary in size, the matching of the non-polar regions is not always perfect. This can be energetically unfavourable and gives rise to several ordering phenomena in the membrane:

- In the simple case of one type of protein and lipids, proteins can form aggregates by themselves, as their hydrophobic length would be equal. Energetically this would be favourable, since only the lipid-protein border will add to the loss of free energy. However, protein function might be reduced or inhibited by close packing.
- In a complex membrane proteins can associate themselves with lipids of similar hydrophobic length. Most likely, the lipid-lipid system will by itself form domains according to hydrophobic matching; proteins will therefore be present in only some parts of the membrane.
- Thermodynamic change of the molecules themselves can occur as another option. Proteins are not rigid and can adopt a structure with a different hydrophobic length. This can have an effect on functionality. Lipids associated to the protein can melt from gel to fluid, reducing the length of their carbon chains. However, this means a loss of free energy and must be outweighed by the gain in increased hydrophobic matching.

As mentioned earlier, physical factors like temperature, pressure and concentration can affect a lipid membrane's physical state. This is also true for lipid-protein system. Depending on the membrane's state of melting, protein hydrophobic matching and function can be affected drastically.

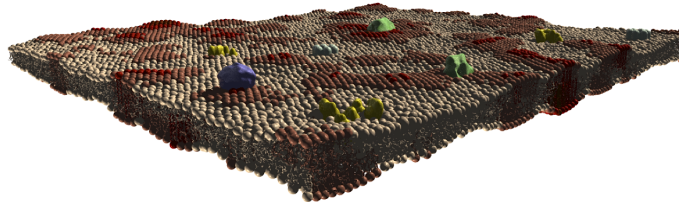


Figure 2.7: Proteins associated with a membrane as imagined in the membrane model of today [6].

# Chapter 3

## Nerves

### 3.1 Structure

The matrix of nerve cells found in a human body and many other organisms lay the base for long-distance signal transmission. Nerve cells, also called neurons, transmit information from and to the brain as well as between each other. A neuron is in its composition very much alike other cells, but its physical size makes it unique. The nerve cell has a cable-like extension that gives it the ability to communicate over long distances in an organism; it is depicted in figure 3.1 and can be divided into the following four parts:

- The soma is the nerve cell's main body and brain. It contains the nucleus and other organelles thereby resembling other cells.
- The dendrites are responsible for handling incoming signals. They are attached to the soma from most sides and scatter out into the nearby tissue in tree-like structures.
- The axon is an elongation of the nerve cell, which is attributed the property of transmitting nerve signals from the point of origin to the destination. The axon length therefore depends on the location of the soma in the body, for humans the longest originates in the foot area and reaches the brain. The axon is usually covered in a sheet of myelin that is produced by the Schwann cells surrounding it.
- The presynaptic terminals occur at the end of the axon and are responsible for transmitting information further on in the nervous system or to the destined tissue.

Santiago Ramón y Cajal showed in the late 19<sup>th</sup> century that neurons were indeed single cells that were not interconnected as previously thought, and

proposed that synaptic signal transmission is based on electrochemical principles. According to the textbook model synapses are present at the tissue-nerve and nerve-nerve interfaces and allow the transmission of information. Certain signaling chemicals with origin in other cells are sensed by the dendrites. This initiates a signal along the length of the axon to its terminal, there releasing other chemicals for the signal to be interpreted accordingly.

The Schwann cells often found along the axon produce a layer of myelin, which has been found to increase the speed of nerve pulses from a few m/s for nonmyelinated nerves to around 100 m/s; given the duration of such signals in the millisecond regime, the physical extension of the nerve pulse can be estimated to be of the order of milli- and centimetres [9].

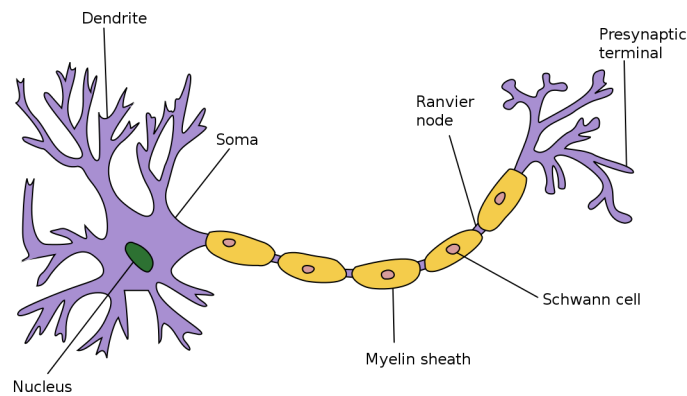


Figure 3.1: A nerve cell and its parts [14]

## 3.2 Hodgkin-Huxley Model

As mentioned earlier, in 1791 Luigi Galvani discovered the "animation" of dead frog's legs by electric stimuli at the spine. This naturally led to the conclusion that nerve signals are of electric nature. It was, however, only in 1952 that Alan L. Hodgkin and Andrew F. Huxley [1] provided a mathematical model to describe the phenomenon.

Hodgkin and Huxley performed experiments with the main giant axon of squids, the reasoning being the sheer physical size of the axon. This led them to propose a model for the signal creation and propagation in nerves. The Hodgkin-Huxley (HH) model is firstly based on the observed ion concentrations inside and outside the nerve cell; potassium ions are found at a concentration of 400 mM inside and 20 mM outside, while the opposite goes

for sodium ions. Secondly, specific transmembrane proteins play a crucial role as channels for sodium and potassium, later denoted as ion channels. These proteins are highly selective of a particular ion type and have a complex voltage and time dependent open-close mechanism. The membrane is considered impermeable to ions and therefore the equivalent of a capacitor.

The idea behind the model is that a local depolarisation will lower the voltage over the membrane and let ions pass through the channels. This flux will further depolarise the membrane and cause more channels to open in the vicinity and conduct ions. This cascade effect acts as the instrument of the propagation of the nerve pulse (Fig. 3.2).

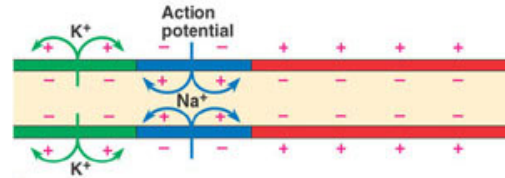


Figure 3.2: Propagation of action potential happening towards the right side of the picture, adapted from [15].

The model can be described as a series of simple electrical circuits, which can be viewed in the schematic of figure 3.3. Though the basic principle is simple, the ion channels' state has a very complex dependence on time and voltage. It must therefore be empirically fitted for any system of interest.

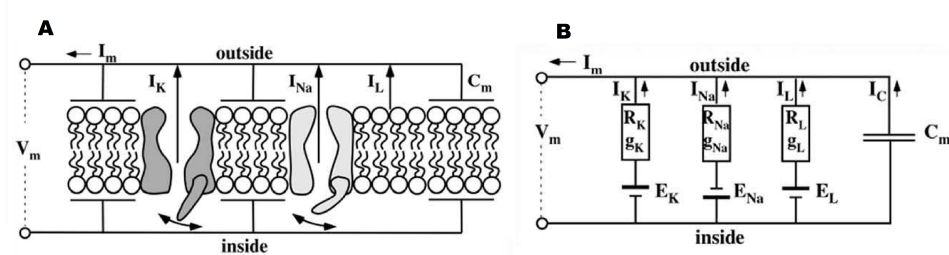


Figure 3.3: *left*, A representation of a piece of axon membrane by the Hodgkin-Huxley model. *Right*, an electrical circuit representation of the same model with resistances ( $R$ ), conductances ( $g$ ), capacitance ( $C_m$ ), currents ( $I$ ) and ionic resting potentials ( $E$ ).

As mentioned above, the membrane is considered to be impermeable and acts as a capacitor,  $C_m$ ; ions on its surface form a voltage  $V_m$  across it.

Therefore, the embedded ion channels can be considered resistors with conductances  $g_K(U, t) = \frac{1}{R_K}$  and  $g_{Na}(U, t) = \frac{1}{R_{Na}}$ . The charge on a capacitor is expressed as following:

$$Q = C_m \cdot V_m \quad (3.1)$$

The HH model assumes the capacitance is constant in time,  $dC_m/dt = 0$ . The current is the temporal derivative of the charge, therefore:

$$I_c = \frac{dQ}{dt} = C_m \frac{dV_m}{dt} + V_m \frac{dC_m}{dt} = C_m \frac{dV_m}{dt} \quad (3.2)$$

And lastly, taking into account the ion channels, the current through a piece of membrane, also called the membrane current, thus becomes:

$$I_m = C_m \frac{dV_m}{dt} + g_K(V_m - E_K) + g_{Na}(V_m - E_{Na}) + \dots \quad (3.3)$$

where potentially more terms can be added to accommodate for other ions. Equation 3.3 is inserted into the cable equation (Eq. 3.4) to get the following partial differential equation. Here,  $a$  is the radius of the axon and  $R_i$  the resistivity along the nerve due to forces in the interior of the nerve cell:

$$\frac{1}{r_l} \frac{\partial^2 V}{\partial x^2} = c_m \frac{\partial V_m}{\partial t} + \frac{V}{r_m} \quad (3.4)$$

$$\frac{a}{2R_i} \cdot \frac{\partial^2 V_m}{\partial x^2} = C_m \frac{\partial V_m}{\partial t} + g_K(V_m - E_K) + g_{Na}(V_m - E_{Na}) + \dots \quad (3.5)$$

With this equation Hodgkin and Huxley could successfully predict and describe action potentials as depicted in figure 3.4. The action potential is the aforementioned localised voltage change that can propagate down an axon. Its function in nerves has made the term almost identical with nerve signals.

Hodgkin and Huxley received the Nobel prize in medicine in 1963 for their model. The idea of understanding the nerve pulse through channel mechanisms has gained a wide acceptance in the scientific community and become the mainstream school. It has also triggered extensive research in channel proteins and even their crystallisation [16]. The HH model is indeed a good model for certain predictions about the squid axon: it describes the nerve pulse and gives an estimate of its speed. Its basics are also easy to understand due to the simplicity of the electrical circuit. However, as the authors mentioned, their findings are just an empirical description of the observable:

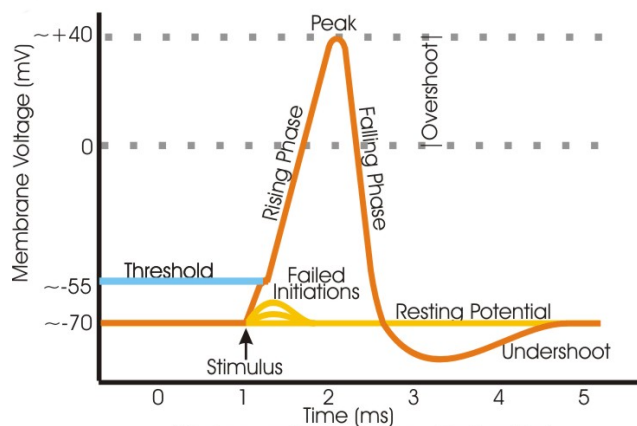


Figure 3.4: Idealised action potential

*"The agreement must not be taken as evidence that our equations are anything more than an empirical description of the time-course of the changes in permeability to sodium and potassium. An equally satisfactory description of the voltage clamp data could no doubt have been achieved with equations of very different form, which would probably have been equally successful in predicting the electrical behavior of the membrane." [1]*

### 3.2.1 Shortcomings of the Hodgkin-Huxley model

There are several phenomena the HH model does not take into account by assuming a static structure for the nerve. By knowing the dynamic nature of lipid systems, one can already see several shortcomings. Lipid membranes are known to be very flexible, especially near and in the phase transition, and indeed Iwasa [17] and Tasaki [18] have shown that the action potential is not only of electrical nature, but is accompanied by a swelling of the tissue and nerve contraction. In fact, studies have indicated the possibility of the membrane going into its phase transition during nerve pulse propagation.

In any real physical system it is also important to take into account thermodynamics, not only the mechanical changes. The HH model relies on channel proteins and currents through them to explain nerve pulse phenomena. In its electrical circuit form resistors play this role. Both cases are by nature dissipative and will release heat. According to Ritchie and Keynes [19], pulse propagation is adiabatic, and heat released during the first part of pulse propagation is reabsorbed immediately after.

Clearly, there are physical aspects of the nerve system that the HH model does not cover. The adiabatic nature of the pulse propagation coupled with the mechanical changes due to internal pressure, resembles a form of density or pressure wave. This analog lead Heimburg and Jackson to the proposal of the *soliton model* [2].

### 3.3 The Soliton Model

As a general principle, physical phenomena should be described by laws that act on the same length scale. The movement of wind in the atmosphere can not be described by the states of single air molecules. Likewise in membranes, the explanation of nerve pulses must lie in the range from millimetres to several centimetres. The density pulses mentioned right above have a striking resemblance to sound waves, and therefore Heimburg and Jackson based their soliton model on thermodynamics and hydrodynamics. [2].

A soliton is a wave or wave packet that travels in a medium, maintaining constant speed and amplitude. The existence of solitons requires a medium exhibiting non-linearity and dispersion: the wave speed has a non-linear dependence on density and is also dependent on the frequency of the wave, respectively. Coincidentally, biological membranes have just these properties in the vicinity of the phase transition.

The soliton model treats nerve pulse propagation as a 1-dimensional problem, since the nerve can be assumed as an infinite homogeneous cylinder. The model is based on the equation for sound:

$$\frac{\partial^2}{\partial t^2} \Delta\rho^A = \frac{\partial}{\partial x} \left( \frac{1}{\kappa_S^A \cdot \rho^A} \left( \frac{\partial}{\partial x} \Delta\rho^A \right) \right) = c^2 \frac{\partial^2}{\partial x^2} \Delta\rho^A \quad (3.6)$$

where  $c$  is the speed of sound ( $c = \sqrt{1/(\kappa_S^A \cdot \rho^A)}$ ), and  $\Delta\rho^A = \rho^A - \rho_0^A$  is the lateral density of the membrane, a function of  $x$  and  $t$ . The lateral compressibility  $\kappa_S^A$  depends strongly on  $\Delta\rho^A$  in the vicinity of the phase transition, and to capture the non-linear behavior the speed of sound can be Taylor expanded to get:

$$c^2 = c_0^2 + p\Delta\rho^A + q(\Delta\rho^A)^2 + \dots \quad (3.7)$$

where  $c_0$  is the velocity in the fluid membrane state far from the melting transition, and  $p < 0$  and  $q > 0$  are Taylor expansion coefficients that can be experimentally determined.

The model further introduces a dispersion term of the form  $h \frac{\partial^4}{\partial x^4} \Delta\rho^A$  to

yield the complete soliton equation:

$$\frac{\partial^2}{\partial t^2} \Delta \rho^A = \frac{\partial}{\partial x} \left[ (c_0^2 + p \Delta \rho^A + q (\Delta \rho^A)^2) \frac{\partial}{\partial x} \Delta \rho^A \right] - h \frac{\partial^4}{\partial x^4} \Delta \rho^A \quad (3.8)$$

where  $h > 0$  is the dispersion constant. The periodic low-amplitude solution ( $c = c_0$ ) for equation 3.8 is  $\Delta \rho^A = \rho_0^A \sin(\omega t - kx)$  assuming  $\omega = vk$ , where  $v$  is the propagation speed of a wave packet. Inserting the solution into equation 3.8, the dispersion relation is obtained:

$$v^2 = \frac{\omega^2}{k^2} = c_0^2 + hk^2 \approx c_0^2 + \frac{h\omega^2}{c_0^2} \quad (3.9)$$

The approximation holds for  $v \approx c_0$ . Equation 3.9 confirms experimental data indicating that the speed of sound increases with increasing frequency. Using equation 3.8 to find a solution for a propagating soliton with a constant velocity, where  $\Delta \rho^A(z)$  and  $z = x - vt$ , Lautrup et al. [20] have shown that the equation has an exact solution for any given value of  $v$ . It has the following form:

$$\Delta \rho^A = \frac{p}{q} \frac{1 - \left( \frac{v^2 - v_{min}^2}{c_0^2 - v_{min}^2} \right)}{1 + \left( 1 + 2\sqrt{\frac{v^2 - v_{min}^2}{c_0^2 - v_{min}^2}} \right) \cosh \left( \frac{c_0}{\sqrt{h}} z \sqrt{1 - \frac{v^2}{c_0^2}} \right)} \quad (3.10)$$

with the minimum possible velocity for propagating a soliton:

$$v_{min}^2 = c_0^2 - \frac{p^2}{6q} \quad (3.11)$$

For pure DPPC this value is approximately 115 m/s, which is close to the value mentioned in section 3.1. From the equations follows that a slower pulse means a large amplitude. The maximum amplitude is given by:

$$\Delta \rho_{max} = \frac{|p|}{q} \quad (3.12)$$

Furthermore, from the equations it also follows that the velocity of a soliton will depend on its energy, showing the significance of the magnitude of the excitation in the soliton model. The HH model in contrast dictates an all-or-nothing mechanism for pulse creation, where pulses are equal after the minimum threshold is reached. Lautrup et al. [21] showed that a soliton can be produced by an arbitrary excitation, meaning that any perturbation of significant magnitude would suffice to create a soliton.

In contrast to the HH model, which is electrical only, the soliton model is mechanical. Solitons push the membrane locally through the melting transition, where a lot of the membrane's properties drastically change, including

thickness and charge density. Being a thermodynamic model, the soliton model includes all thermodynamic effects, mechanical changes, heat production etc. Heimburg and Jackson [22] have used it to predict the effect of anaesthesia on nerves pulse propagation, showing that the change lies in moving the melting temperature of the lipid membrane.

The effect of an electric field is another way to alter the melting profile of the lipid membrane. This means that a soliton in the lipid membrane will show an electrical component. The electro-mechanical coupling is however not fully known. This thesis will use atomic force microscopy to measure the change in thickness of a membrane exposed to an electric field. This will help map the electrical part of the thermodynamic properties of lipid membranes and their phase transition.

# Chapter 4

## Materials and Methods

### 4.1 Materials

#### 4.1.1 Chemicals

For this thesis the following chemicals have been used:

- 1,2-Dipalmitoyl-sn-phosphatidylcholine (DPPC) obtained from Avanti Polar Lipids in powdered form with molar weight  $M_r = 734.05$  g/mol and melting temperature  $T_m = 41^\circ\text{C}$ .
- 1,2-Dimyristoyl-sn-phosphatidylcholine (DMPC) obtained from Avanti Polar Lipids in powdered form with molar weight  $M_r = 677.94$  g/mol and melting temperature  $T_m = 23^\circ\text{C}$ .
- 1,2-Dilauroyl-sn-phosphatidylcholine (DLPC) obtained from Avanti Polar Lipids in powdered form with molar weight  $M_r = 621.83$  g/mol and melting temperature  $T_m = -1^\circ\text{C}$ .
- 2,2,2-Trifluoroethanol (TFE) obtained from Fluka Analytical of 99.0% purity and molar weight  $M_r = 100.04$  g/mol.
- Dichloromethane obtained from Emsure® of 99.8% purity and molar weight is  $M_r = 84.93$  g/mol.
- Methanol obtained from Uvasol® of 99.9% purity and molar weight  $M_r = 32.04$  g/mol.
- Ethanol obtained from Kemetyl of 96% purity.
- Ultrapure water from the Easypure RF compact ultrapure water system, reaching a resistance of  $18\text{ M}\Omega/\text{cm}$ .

- Loctite® *Circuit+*, a conductive paste with silver particles.
- Loctite® *Activator*, an marker providing better adhesive properties for a layer of glue.
- Loctite® super glue.
- Dow Corning high vacuum grease.
- Nitrogen and air streams

### 4.1.2 Equipment

The following equipment has been used:

- Indium tin oxide (ITO) covered borosilicate glass plates obtained from Präzisions Glas & Optik GmbH. Their thicknesses were 0.8 mm. They were squared with a 2 cm side length.
- Graphene covered silicon dioxide plates obtained from Graphene Supermarket. Their thickness was 0.285 mm. They were squared with a 1 cm side length.
- Muscovite mica crystal flakes obtained from Electron Microscopy Science. They were round with a 9.5 mm diameter. They initial thickness was 0.15 – 0.21 mm.
- AFM cantilever BL-RC150VB-C1 from Olympus. Two V-shaped tips with an 0.006 N/m spring constant made of silicon nitride with gold reflective surface.
- AFM cantilever OMCL-RC800PB-1 from Olympus. Four pyramidal shaped tips with spring constants between 0.06 – 0.82 N/m made of silicon nitride with gold reflective surface.
- Parafilm - a highly elastic film.
- A variety of pipette sizes with glass and plastic tips.
- Vacuum chamber with pump.

## 4.2 Differential scanning calorimetry

As calorimetry is not the topic of the thesis, but only used as a tool, the differential scanning calorimeter (DSC) will only be introduced briefly.

### 4.2.1 The basics

Calorimetry measures heat during chemical or physical changes of a system. Different calorimeters exist that measure heat change under different conditions, but for biological purposes the isothermal titration calorimeter (ITC) and the DSC are primarily used. Only temperatures between 0 and 100°C are required, but the calorimeters are required to be very sensitive, because material can be very precious.

DSC makes use of two cells containing the sample and a reference. Solutions are made in pure water or buffer. The two cells are heated by finely regulated Peltier units, and the temperature is held constant. A sample will require more heat in order to keep the same temperature, because any form of transition requires additional energy. The instrument records the difference in power usage by the units as a function of temperature.

For this thesis the VP-DSC Calorimeter from MicroCal was used, which operates at constant pressure of approximately 50 psi. Pure lipids and lipid mixtures were investigated to find an acceptable concentration. Inspiration was taken from Heimburg [23].

### 4.2.2 Operation

Samples for DSC investigation were aqueous solutions of lipids. Stock solutions in 2:1 dichloromethane:methanol were initially created as further described in section 4.3.3 and appendix A. They were mixed if required, dried under a stream of air and an application of heat and then put in a vacuum bell to deprive the sample of all solvent. Samples were then hydrated in ultrapure water to produce 10 mM aqueous solutions and sonicated for 15-30 minutes until clear. The concentration of material for use in DSC experiments was high compared to the AFM experiments simply because it produced reliable results. Samples were degassed for 10 minutes to make sure no bubbles were present as they would give incorrect results. The sonicator could easily add air to the sample.

The DSC cells were cleaned with alcohol and then ultrapure water for 5-10 minutes each. They were then filled to the brim with their respective content ( $\approx 1$  ml) and sealed. Quick scans could be performed at 40 K/h to locate a smaller temperature range to scan more closely, but the data presented in section 5.1 have all been scanned at 5 K/h for precision.

### 4.3 Atomic Force Microscopy

Atomic Force Microscopy (AFM) is a powerful imaging technique from the family of Scanning Probe Microscopes (SPM) that allows the user to measure the surface structure of a sample at atomic resolution [24]. The feature SPMs have in common is the use of a probe or tip that can be moved laterally over a sample, typically both in  $x$ - and  $y$ -directions, relying on interactions between the probe and the surface to inspect the topography of the latter. In this sense, these techniques differ from other types of microscopy by not focusing light or electrons through the sample to be read by a sensitive surface; instead, they physically "feel" the contours. No lensing effects and no illumination is used on the inspected sample.

The history of SPM dates back almost a century, to 1929, when Schmalz described the *stylus profiler* [25]. This instrument possessed a sharp tip that was dragged over a sample, following its contour, much like the mechanism of a gramophone. A mirror at the tip was illuminated, and redirected the incoming light onto photographic paper. Common problems with the profiler were the bending of probes when encountering large surface features, but also the invasive nature of it, which could destroy a sample. The former was addressed already in 1955 by Becker [26], suggesting an oscillating motion of the probe, where it always would approach the sample from above.

Notable improvements were presented by Young [27] in 1971 with his *typografiner*, which used piezoelectric components for probe movement. A feedback loop over the electron field emission from probe to sample was used to control the distance between them. This was further perfected by Binnig and Rohrer [28], who invented the Scanning Tunneling Microscope (STM) in 1982. This instrument's improved sensitivity over the typografiner was the result of electron tunneling driving the feedback loop. Electron tunneling occurs at near-contact, and only the outer most atom of the tip is included in the process, meaning that the tip's form further away from the sample is almost irrelevant. Binnig and Rohrer received the Nobel prize in 1986 for their work.

Although creating a breakthrough, the STM's shortcoming was in its limitation to conductive samples. However, already in 1986 the invention of the AFM by Binnig, Quate and Gerber [29] followed. As the stylus profiler, the AFM presses its tip over the sample. Sensors monitor the interaction and adjust the force on the tip to keep the procedure non-invasive. In modern designs piezoelectric elements are used in this feedback loop, while a laser's reflection from the cantilever is used to record the height sensed by it. A detailed explanation is found in the following section.

A very strong argument in favour of AFM is its wide variety of applica-

tions [30]. It can be used in a multitude of environments: in vacuum, in gas and in liquid; in a temperature range from cryogenic to well above room temperature<sup>1</sup>; and on nearly any hardness of sample: ceramics, metal, polymer materials, biological cell tissue and DNA. Wonderful examples of its use are for example the depiction of the location of carbon atoms in sheet carbon material and the imaging of several bacterial cells at once [31].

This chapter will explain the use of the AFM technique for biology and for biological membranes in particular.

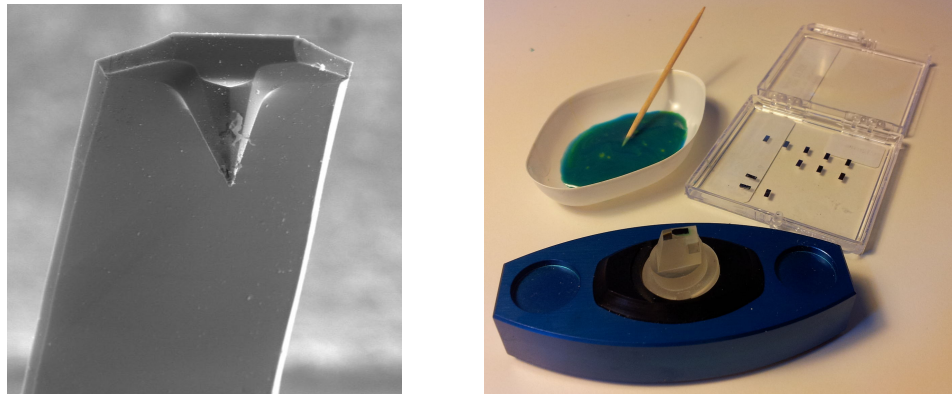
### 4.3.1 The microscope

The AFM used for this project is the NanoWizard II from JPK Instruments. Other microscopes of course work by similar principles, but the following describes this one in particular. The setup of the AFM includes a number of different elements. First of all there are the microscope mechanics. As mentioned above, AFM uses a *tip* to map the surface contours of a sample. The tips are located at the end of a *cantilever*, which extends out from a *chip*, Figure 4.1a. The cantilevers and tips are made out of Si or SiN with a gold or aluminium coating on the top side to reflect the laser. Different shapes and dimensions of both are mentioned in Figure 4.1a and provide for different properties: the force constant and the resonance frequency; which affect the precision and resolution of measurements. For the biological samples in this thesis softer tips were chosen, as they provided for a more non-invasive scanning as well as stability of the sample. The samples were fragile, but needed to remain stable for longer periods of time in a turbulent environment and the measurements needed therefore be as delicate as possible.

This chip is mounted on the AFM *cantilever holder*, which is a glass block that has been optically polished on top and bottom sides to let a laser beam through, Figure 4.1b. The chip is attached to the holder using a rubber-like biodegradable two-component glue. The holder is placed and fastened in the AFM *stage*, which encompasses all the electronics: the laser beam hitting the cantilever, the photodiode recording the deflection of the beam, the sensors that read the interactions of the tip with the surface and the piezomotors that govern the movement of the system in the  $x, y, z$ -directions, Figure 4.2. The sample is located below the AFM stage, and in our setup there is further connected an Olympus IX71 inverted optical microscope with an ImagingSource DFK 31AF03 colour camera from below. The whole setup is placed on an active anti-vibrational table, the TS-150 from Table Stable,

---

<sup>1</sup>This will depend on how high a temperature a given sample can be exposed to without being damaged



(a) Cantilever with tip [32]

(b) Cantilever holder, several chips and rubber glue

Figure 4.1: Parts of the AFM setup.

which in turn resides on an optical table from Thorlabs.

The AFM stage is connected to a large computer that handles the input and output. Apart from interpreting signals from the AFM stage, the computer can be supplied with further input, such as a voltage signal, in order to superimpose datasets. The large data handler is controlled by the user via the supplied NanoWizard SPM software running on a Debian Linux operating system.

### 4.3.2 Operation

In order to successfully image a surface with the AFM, there are a few steps to follow. Firstly, under a simple light microscope one attaches the chip with the cantilever to the cantilever holder. The cantilever holder is put in a special stand, so it is not damaged or scratched on either side, remember that both sides have optically polished glass surface. A droplet of a rubber-like two-component biodegradable glue is administered on its "rough" part. Using a fine set of tweezers the chip is placed on top of the glue, while the cantilever(s) extend over the polished part, see figure 4.3a. The cantilever tips will actually point upwards, since this is the bottom part of the setup. After drying, the holder is attached in the AFM stage.

The laser is to hit the outer most part of the cantilever. This is where the cantilever will move the most in the  $z$ -direction. As illustrated in figure 4.4a, it is necessary to adjust the mirror and the detector in order for the laser beam to hit the exact center of the detector. This is a tricky procedure, but one gets better at it with time. For course adjustment one tilts the mirror until

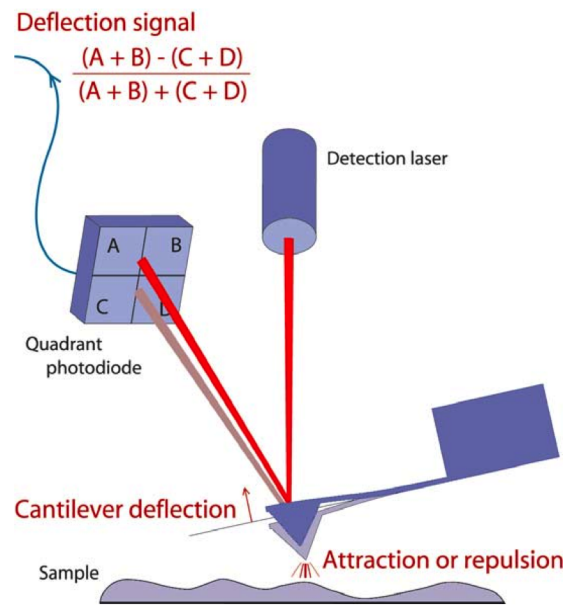


Figure 4.2: The main parts of the AFM system, the cantilever, laser and detector, responsible for imaging [33].

the red spot in the laser alignment window (Fig. 4.4b), symbolising where the laser hits, is visible inside one of the four quadrants. Then one adjusts the position of the detector to center the laser spot. The desired values for imaging are approximately 0 vertical and lateral deflection, meaning that the laser is centered, and a sum of above 1V.

Coarse adjustment is required when changing between air and water as the medium due to refraction at the interface and the alteration of the laser's path. It can also be required if a new cantilever has very different geometry. For similar cantilevers one will only need to readjust the detector.

In case of failed alignment there are several things to check. The laser can be realigned to hit a slightly different place on the cantilever. If one is still unsuccessful, most likely the chip is placed in a way that alignment is impossible. The chip and cantilever could be tilted or not sufficiently exposed, preventing a laser path to the detector to be clear. Glue might also have spread to block the path. Reattachment of the chip to the holder is necessary.

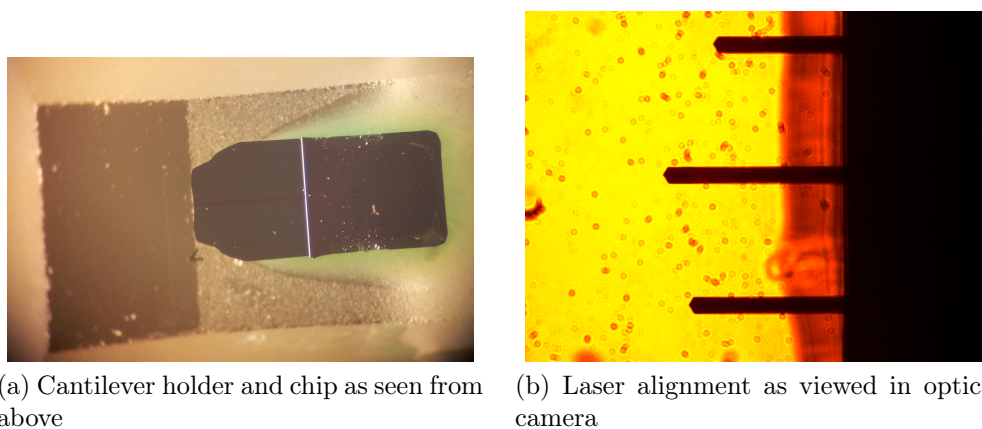


Figure 4.3: Different view of the cantilever. The left picture providing the optical view is used to position the laser on the cantilever.

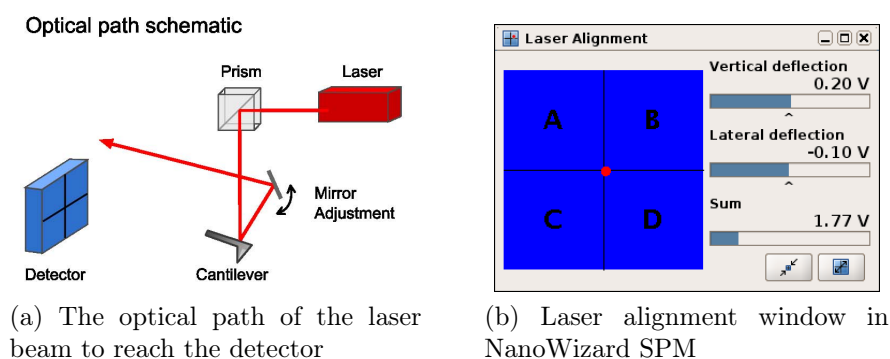


Figure 4.4: Laser path adjustment [34]

## Scanning modes

When laser alignment is successful the sample is placed under the AFM stage and approach can begin. The two modes used in this project are contact and intermittent contact modes, figure 4.5. As described above, in contact mode a probe keeps a close fixed distance to the sample, while in intermittent contact mode the probe constantly retracts for a more delicate treatment of the sample. Force modulation mode was a third possibility with the instrument, in which the probe does not leave the surface, but this was not used.

For contact mode the approach of the tip to the sample is straightforward and requires just a press of a button. For intermittent contact mode a few specifications have to take place with regard to the cantilever initially. First

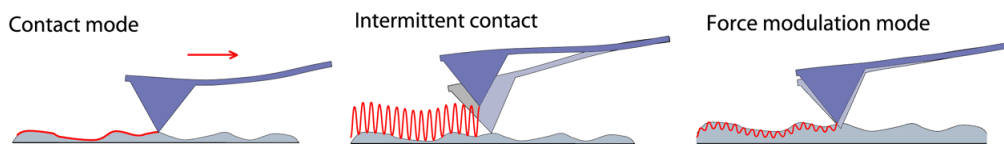


Figure 4.5: Different AFM scanning modes [33]

of all the choice of cantilever for intermittent contact mode depends on the medium it is to be used in. In air a stiff cantilever (high spring constant,  $k$  value) with a high resonant frequency is used. In water, softer cantilevers should be used, 0.3 N/m will do. Secondly, the cantilever should be tuned, and the correct frequency chosen, in which it will operate. This frequency will also be provided by the manufacturer of the cantilever.

For both modes approach parameters and feedback control must be set. A setpoint must be chosen, which decides the force used whilst imaging. The higher force used, the higher probability of damaging the sample. These parameters have changed from sample to sample and from scan to scan to obtain the best results. Approach can be done coarsely initially to save time.

Imaging options that have been used and varied are scanning area, resolution and speed. The latter can be altered in both  $x$  and  $y$  directions.

### 4.3.3 Sample preparation

Throughout this thesis DLPC, DMPC and DPPC have been used for imaging and investigation. They were stored at minus 25°C. Each time any substance was taken out of the freezer for use, it was kept sealed and closed until reaching room temperature. This prevented condensation of water on the inside of the respective container. Sample preparation for the AFM consisted of three parts: the preparation of the lipid stock solutions, the solutions to be used for imaging and the deposition of the solutions onto a substrate<sup>2</sup>.

Stock solutions were made by dissolving the respective lipid, a white powder, using 2:1 dichloromethane:methanol as solvent. Typically, the desired concentration to reach was about 10 mM, so 20–25 mg of lipid were dissolved in 3.2 – 3.5 ml of solvent. The flasks used could contain up to 4 ml. The solutions were then sonicated, sealed with Parafilm, and put in the freezer for storage.

To create a sample for deposition, the stock solutions were mixed in desired proportions or kept as is. A small portion was repipetted into a new

<sup>2</sup>A detailed procedure can be found in the appendix.

vial, which was dried under an air stream while being heated at approximately 50°C. They were then further deprived of solvent in a vacuum bell. The now dry lipids, a thin layer of white powder on the bottom, were redissolved in a fitting amount of millipore water or TFE. In case of the former, the solution was sonicated using a Branson analog cell disruptor. During the sonication the solution went through a milky-white state to a clear one; the time required was at least 15 minutes. The concentration of the samples used in the experiments was typically in the range of 0.1 – 1 mM and the procedure was adjusted to produce these concentrations. The samples were, likewise, stored airtight in the freezer.

The last step largely depends on the complexity of the experiment. Three different support materials have been used as described in 4.1.2: mica, ITO covered glass and graphene covered glass. Mica was glued onto a glass slide for support. Graphene plates were super glued onto ITO plates as their smaller size could not be used for the setup. Silver glue created a conducting link between the two. Samples dissolved in both water and TFE were pipetted onto their respective plates and put in the vacuum bell for at least a few hours. Although TFE evaporated almost instantly upon deposition, the vacuum bell was used to remove any remaining solvent, which would otherwise give erroneous results. Water-based samples were initially heated at 40-50°C to increase evaporation speed.

For experiments in air no further preparation was needed; the samples could be put under the microscope. For experiments in water, after being exposed to vacuum the samples were glued onto a small chamber that held the water (Fig. 4.6). Vacuum grease was used for attachment. The chamber had electrodes on its top and bottom, which allowed for an external electric field to be applied over the water in the  $z$ -direction. The chamber was screwed into a brass block (Fig. 4.6) for stability, which had the additional function of serving as a water bath.

#### 4.3.4 Cleaning procedure

When mentioning water in this section the writer refers to ultrapure water.

ITO plates were cleaned between experiments by hand using a soft tissue and ethanol and water several times. After the last administration of ethanol tissue is not used, and instead the ITO plate is dried under a stream of nitrogen. The vacuum grease was the difficult part to remove, not the lipids.

Graphene plates are more fragile and were soaked in ethanol for short periods of time initially, then carefully followed the procedure like the ITO plates. Since vacuum grease was not used directly on the graphene plates due to their size, they were not complicated to clean.



Figure 4.6: Experimental sample setup. The samples are attached to the inner plastic chamber from below, a square of metal is attached from above. Both have an electric connections to the electrodes sticking out. The chamber was screwed onto the brass block for stability and temperature regulation.

Sample vials are washed and dried by machine, but still given a few sprays of ethanol and water and then dried under nitrogen. Plastic and brass components follow same procedure.

The AFM glass cantilever holder does not need to be cleaned often, but can be if needed. If is put holder-side down in water on a provided raft. Water is also pipetted on the larger flat side from the top. A small amount of dishwash is added to the water. Then a sonication is applied. After an appropriate time the holder is removed, washed clean by water and dried.



# Chapter 5

## Results and Discussion

In this chapter the results obtained during the experiments will be presented. It will be structured as a learning process with increasing complexity of experiments both to make it easier for the reader to understand the obstacles that can arise, but also as a guide or reference to be used for planning a similar project using an atomic force microscope. The reader is presented with single cases from experimental series with lipids<sup>1</sup>; comments and discussions accompany each set of results.

### 5.1 Calorimetry

This section presents data obtained with the DSC. Both pure lipid solutions and mixtures of different lipids have been used for calorimetric analysis. The goal was to verify and choose a lipid mixture for use in the AFM experiments with a phase transition spanning biological temperatures from below to above room temperature; the AFM experiments fixed the temperature of the setup at 23°C with a water bath. A single lipid species has a very narrow phase transition. However, for this thesis a gradual change in the lipid membrane is desired, as it is easier to work with. A broad transition can be achieved by mixing two different lipid species, and the phase transition of the combined mixture will span a temperature range somewhere between the two extrema, the exact values defined by the mixing ratio.

The raw data was subtracted a baseline and adjusted for lipid concentration in IgorPro.

The images 5.1-5.3 show melting profiles for DPPC, a 65%:35% DPPC:DLPC mixture and a 70%:30% DPPC:DLPC mixture, respectively. They illustrate the difference between the sharp melting profile of a pure lipid membrane

---

<sup>1</sup>The terms layer, lipid layer, bilayer, membrane are used interchangeably.

and a broad transition, and also how a slight change in mixture ratio can play a role on the melting profile.

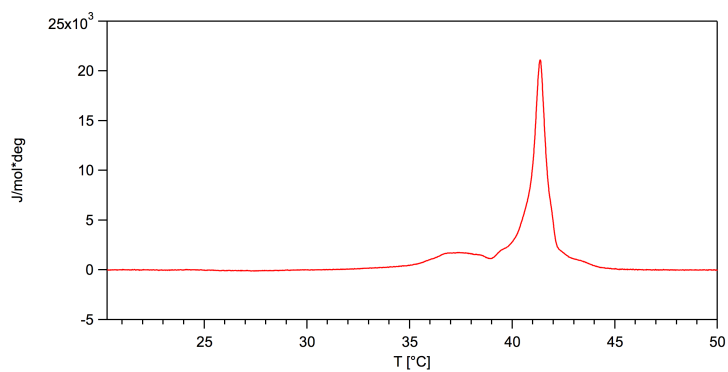


Figure 5.1: Calorimetry scan of pure DPPC.

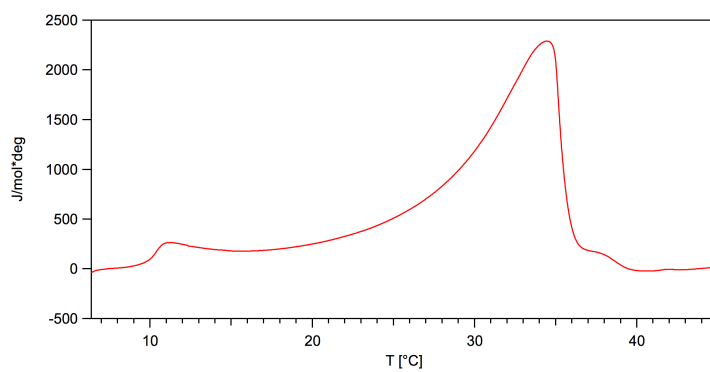


Figure 5.2: Calorimetry scan of a 65%:35% DPPC:DLPC mixture.

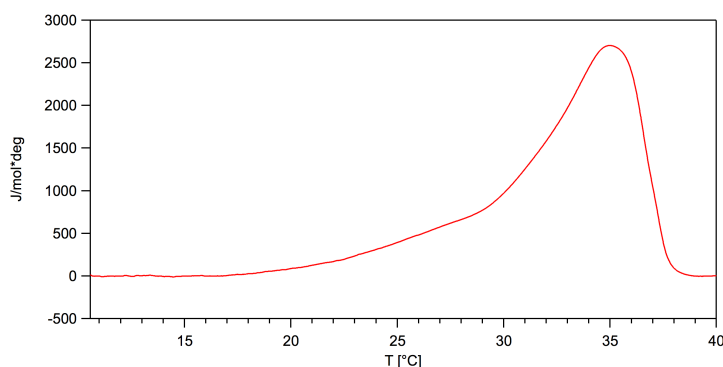


Figure 5.3: Calorimetry scan of a 70%:30% DPPC:DLPC mixture.

## 5.2 Atomic force microscopy

Raw images obtained using AFM were treated and corrected using the open source Gwyddion software version 2.28 [35], which is an advanced program for SPM image analysis and visualisation. AFM images are presented with a colour hue height scale next to them, which not always begins at a zero point; this happens, because the scale is chosen to create a proper amount of contrast in the images for the reader to distinguish surface features. Many images also have marked profiles of membrane thickness, which are presented on graphs that accompany them.

Sample preparation is a very important part of working with the AFM. Samples for this thesis were prepared from pure solutions or mixtures of DLPC, DMPC and DPPC dissolved in TFE or ultrapure. As mentioned in section 4.3.3, a part of the procedure was the use of a vacuum bell for complete solvent removal, which added a lot of time to sample preparation. Therefore, to save time, labour and materials during the project, the goal of the initial experiments was to find a method to deposit the proper amount of material onto the plates. This was done by varying the concentration and volume of the pipetted solutions. Multiple depositions were also tried.

An important thing to note about the AFM before beginning is its sensitivity. Vibrations can easily distort an image, therefore walking, talking and the use of doors should be kept at a minimum.

### 5.2.1 Experiments on mica in air

Initially water-dissolved solutions were used for experimentation. After several trials, a 10  $\mu\text{l}$  of a 100 nM solution was found to produce the desired results. This amount and concentration is only to be taken as a guideline as

lipid deposition varied over long distances; large areas had to be scanned to find optimal locations for more precise scans. The ratio of mixture of 65% DPPC to 35% DLPC was chosen in order for room temperature to be located in the middle of its broad phase transition [23]. Piece of mica were glued onto glass slides for stability. In these experiments a droplet of solution was placed on the mica and heated slightly for faster evaporation.

Figure 5.4, however, shows one of the issues of having excessive material deposited: the surface of the plate, to be used as reference point, is very difficult or impossible to find. Observations showed that an abundance of lipid layers also made it impossible to estimate their exact amount due to variations in height of every layer. This happened because layering would not occur in a strictly quantified manner, but with overlaps.

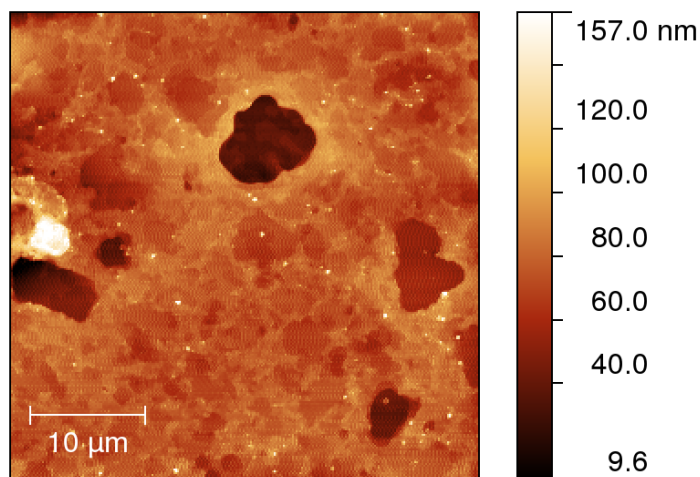


Figure 5.4: A scan of a large area of a 65:35 DPPC:DLPC mixture on mica in air

Figure 5.5a shows a limited amount of *pure* DPPC on mica. The mica plate is clearly visible, and mostly single bilayers are found with a few occurrences of a second bilayer on top of the first. Figure 5.5b shows a clear-cut distinction of the two layerings and the homogeneity of the corresponding heights. The height of the DPPC bilayers was found to be approximately 6 nm in accordance with [36].

In contrast, figure 5.6 again shows excessive amounts of lipid material, though on a smaller scale than in figure 5.4. Profile 1 spans almost 4  $\mu\text{m}$ , still showing clear height difference from one layer to another, while profile 2 goes through the only reference point in the picture, where no material is found.

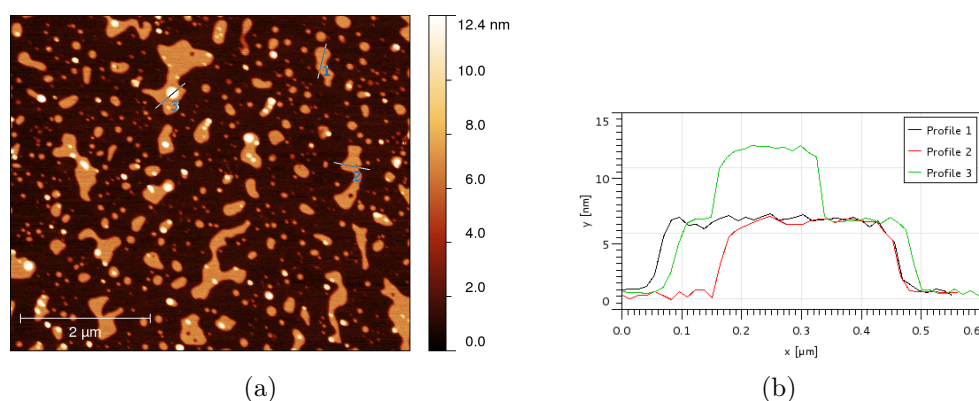


Figure 5.5: Figure *a* shows a scan of a pure DPPC on mica in air. Many pieces of membrane are visible. *b* shows the heights of the profiles selected in *a*.

Note that these experiments were done at room temperature, where a pure DPPC membrane is in its gel state. Clear-cut results similar to figure 5.5 were therefore easily obtained. However, a mixture of lipids has a broad transition, and variations in height were spotted already at this stage. It is only slightly visible in figure 5.6b, but much more so in 5.7b. These differences depend on the localised state of the membrane, which in turn is affected by temperature and localised concentration proportions of the lipids.

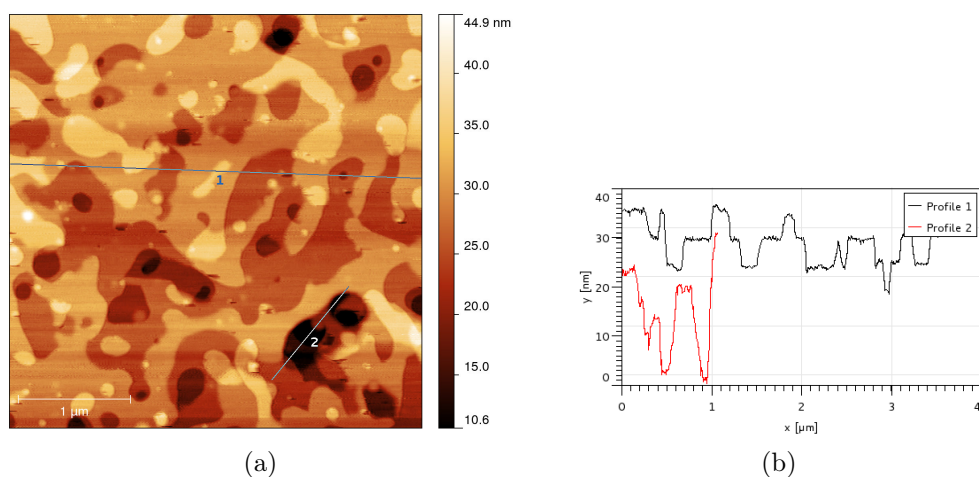


Figure 5.6: Figure *a* shows a scan of a 65:35 DPPC:DLPC mixture on mica in air with a noticeable number of lipid membranes piled on top of each other. Figure *b*: profile 1 transverses the whole picture, while profile 2 goes through a zero reference point.

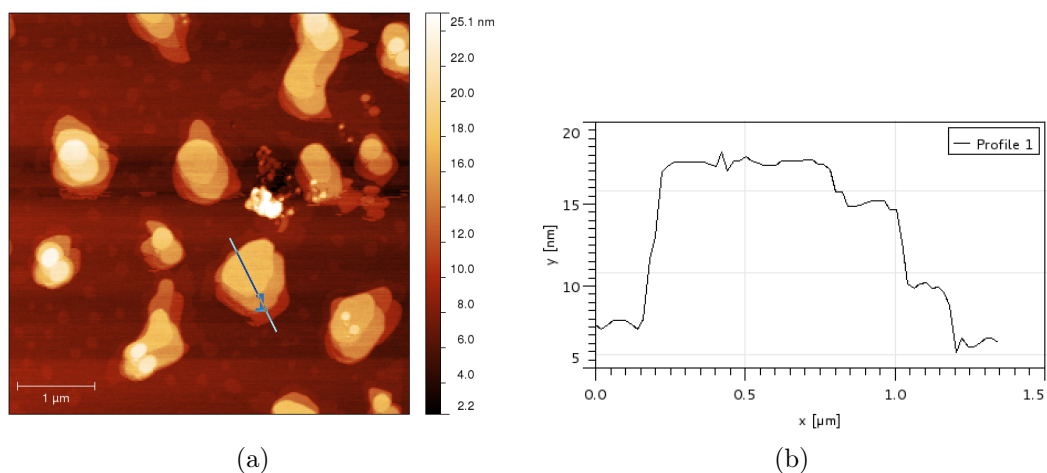


Figure 5.7: A 65:35 DPPC:DLPC mixture on mica in air with thickness profile.

### 5.2.2 Experiments on mica in water

Increasing the complexity of the experiments, water was pipetted onto the samples and put in the setup mentioned in 4.3.3. Figures 5.8 and B.1 show how DPPC still settles in bilayers on the mica's surface exhibiting no change in height. The DPPC-DLPC mixtures were less comparable to their counterparts in air. Their distribution of heights was not as discrete.

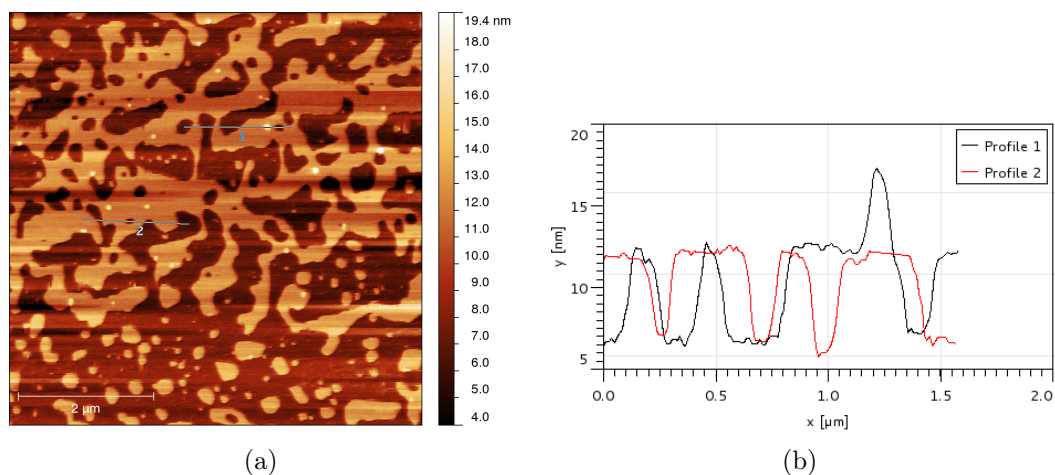


Figure 5.8: Pure DPPC on mica in water with thickness profile.

The addition of water in these experiments is believed to have opened up for much freer fluctuation and movement of the molecules. Furthermore,

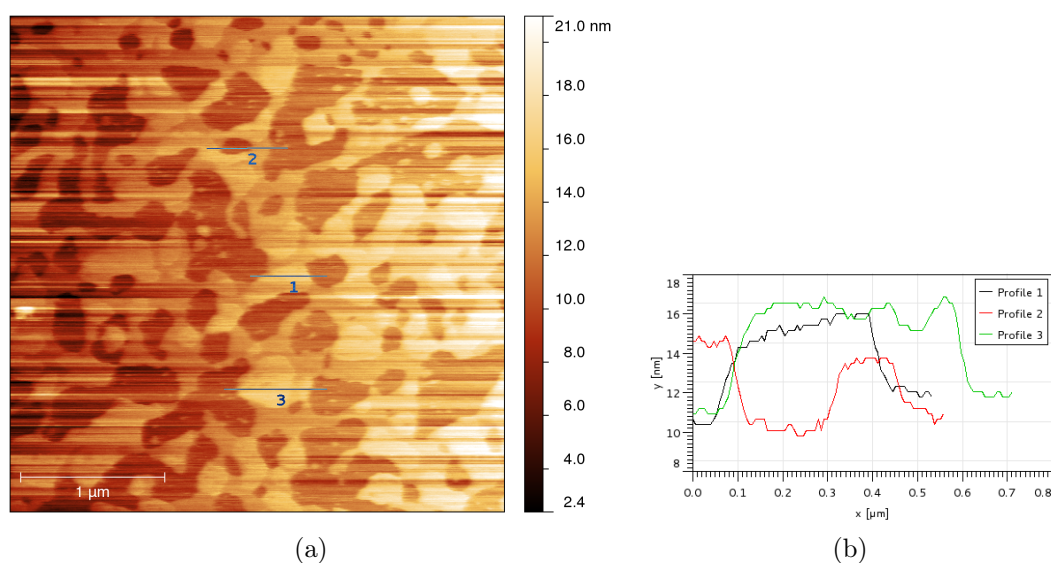


Figure 5.9: A 65:35 DPPC:DLPC mixture on mica in water with thickness profile.

water has previously been shown to incorporate itself between lipid bilayers [37], increasing the measured height of a second or higher number bilayer by 2 nm. This interaction could also be a reason for less uniform lipid layers in the experiments even though they show a single layer.

### 5.2.3 Experiments on ITO in water

The experiments on mica were intended as a trial, because mica displays a very flat surface that helps the formation of uniform lipid membranes. During this period the operation of the AFM and sample preparation became a habit. These trials were a tool to explore the dynamic system that is biological lipid bilayers and to get the writer accustomed to working with them. Mica made an easy platform in this sense due to its flatness.

Mica, however, is not conductive. The further course of the thesis required a conductive surface to be covered with lipid bilayers to investigate the effect of an external voltage on the membrane. This meant that the next step was to use indium tin oxide covered glass plates as substrate for experimentation.

An ITO covered glass plate proved to be a tricky surface to work with because of the irregularities of the glass and in turn the ITO. Initial results proved to be undesirable. The lipid domains were very small and cluttered, figure 5.10. It was also very difficult to find a proper reference point to the surface. Scanning smaller areas, increasing resolution or lowering speeds also

proved a failure. Changing concentration only meant that these regions were scattered or that no structures of significance formed at all.

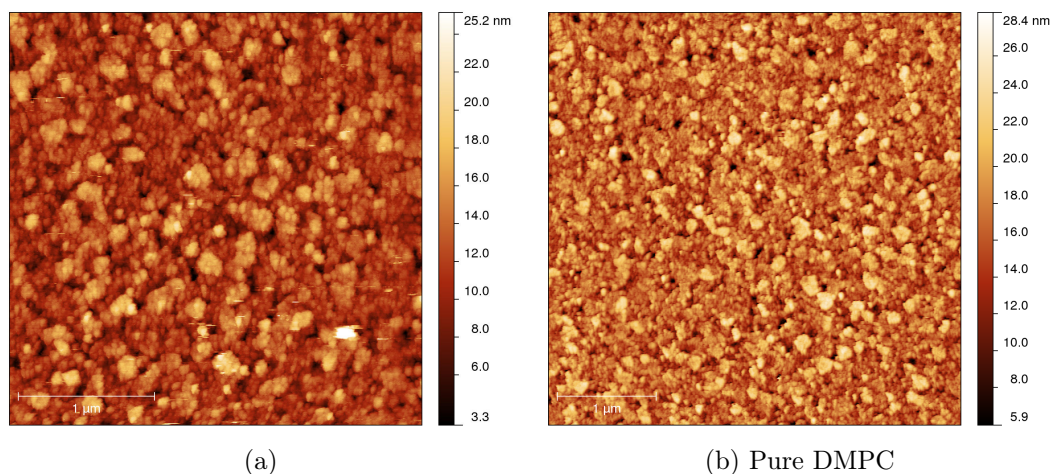


Figure 5.10: Initial results on ITO covered glass plated in water. Figure *a* shows a 65:35 DPPC:DLPC mixture, while figure *b* shows pure DMPC.

The ITO plate itself was examined. Although it was known that the surface of an ITO is highly irregular, the tall features that were found (Fig. 5.11) were astounding. The ITO's surface had fluctuations on the scale of a lipid bilayer and visually it could indeed be mistaken for one. To be sure, this was repeated with a completely new ITO plate, leaving out the possible error of residual lipids from previous experiments. A very large scan of the background roughness can be seen in figure B.3. A new approach had to be considered.

#### 5.2.4 Experiments on ITO using TFE as solvent

The sample preparation method came into question: could a lipid solution in water deposit the lipids in a desirable manner on an ITO? TFE was chosen as solvent for further experiments. After the removal of solvent in a vacuum bell, samples required rehydration. This was done under a lid at around 50°C in a moist atmosphere. Water was pipetted to cover after the sample had been fixed in the setup. The samples ranged between 4 – 6 μl and were typically 1 mM.

Using this approach the results improved substantially. A TFE-dissolved sample on an ITO surface in air provided some of the most beautiful long-scale images acquired (Fig. 5.12, B.4). In figure 5.12b one can still see the

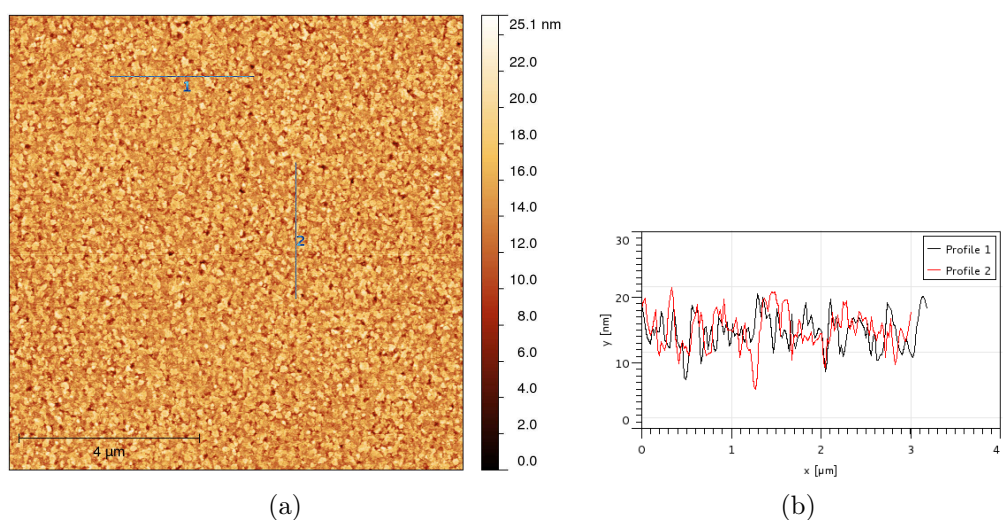


Figure 5.11: The ITO background and respective profiles.

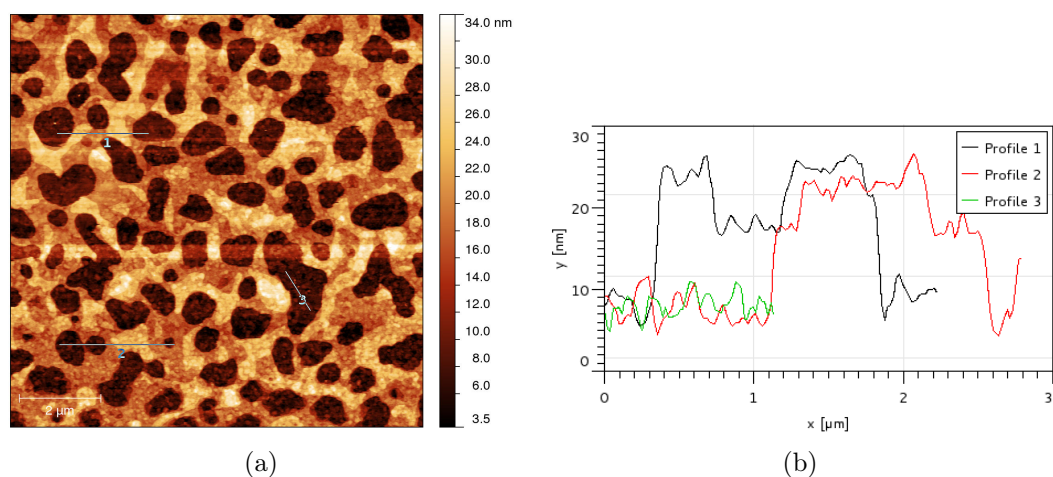


Figure 5.12: TFE-deposited lipids on and ITO surface in air.

rough background of the ITO, but it has been considerably smoothed. When deposited in a solvent instead of water, the lipids could fill out the roughness of the ITO providing for a smoother surface. In water results were still not ideal, as seen in figure 5.13. However, the results displayed areas of membrane well-defined enough for further experiments, and it was decided to progress with applying an external electric potential over the created lipid bilayers and analyse data from obtained results, which was the aim of the thesis.

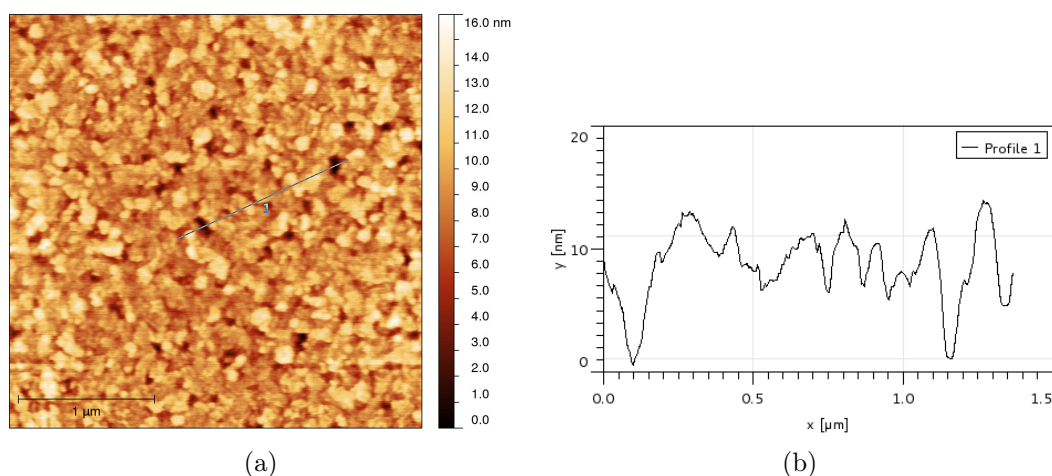


Figure 5.13: TFE-deposited lipids on and ITO surface in water.

### 5.2.5 Experiments on ITO with an external electric field

A voltage generator was attached to the electrodes (Fig. 4.6) and an area of the sample for scanning was selected. While it was possible to find areas acceptable for imaging, where membrane layers were observed, they were not ideal due to the lack of flat areas on the ITO support.

Another complication was discovered that wasn't observed during previous imaging. A single scan took 10-20 minutes depending on the parameters chosen; therefore, a set of readings at different voltages could take a few hours depending on the amount of images at each step and relaxation time after voltage switch taken into account. Over the course of this time the deposited lipids were observed to move in a particular direction. Furthermore, sometimes instances of membrane would collapse or be washed away. These effects could result from an error caused by the microscope, or because the lipids were not properly attached to the surface, since they rested on an rough surface of ITO filled out by lipid material. Currents of water might also have been responsible, but a more likely reason was thought to be the increased mobility of the membrane, when it became more fluid.

Fluctuations in the aqueous environment also meant that even two images taken in succession of each other would give slightly different results with respect to membrane height. Therefore, the writer strove to make several images at each instance of applied voltage, keeping in mind that a sample's lifetime was limited.

The following figures present the data obtained by altering the electric field in the system. Temperature was kept constant at 23°C. Averages of data obtained from trace and retrace images were used and from several

images, where possible. The images were not very clear and therefore small areas could not be used for data collection; instead, the whole image was used. As the presented data is gathered from different samples, the height of the membrane at 0 V for each sample is taken as baseline for the particular profile, and height change is presented as a percentage change with respect to that for comparison. The profiles seen in figure 5.15 belong to images 5.14a, 5.14b, while the profiles in figure 5.16 are of 5.13a. All were a mixture with 65:35 DPPC:DLPC lipid ratio.

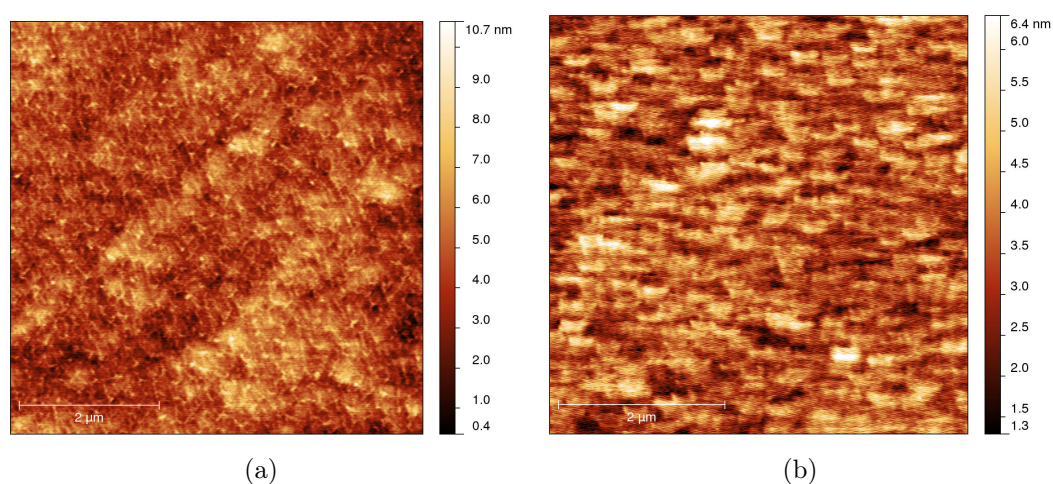


Figure 5.14: Two of the samples used for data collection.

Judging from figures 5.15 and 5.16 there is no doubt that the lipid bilayers are affected by the applied voltage. Their frantic behaviour, however, can only hint towards a general direction in the results. The membranes tended to become thinner while being exposed to low voltages, but then rising in thickness as voltage went up, this will be discussed below.

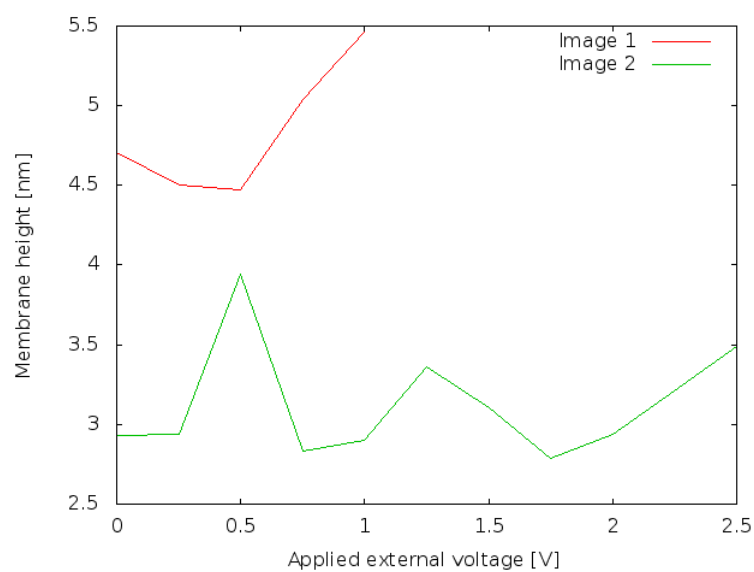


Figure 5.15: Results obtained from ITO experiments with low voltage from two different images.

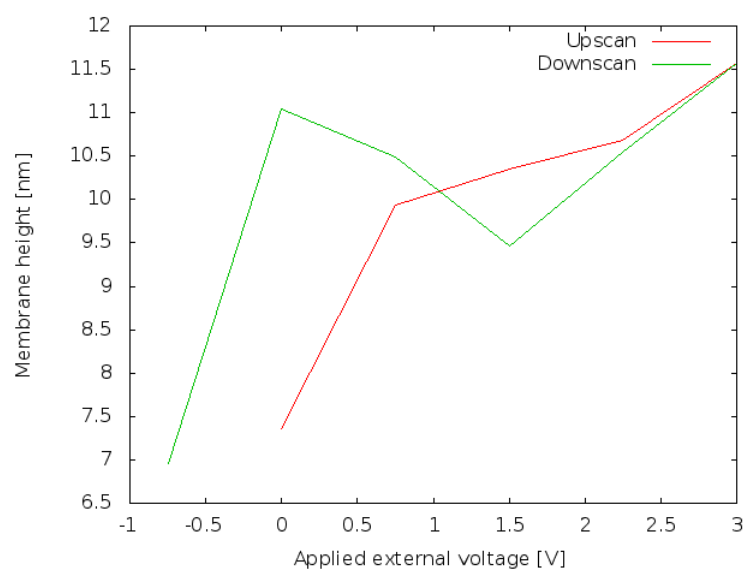


Figure 5.16: Results obtained from ITO experiments with high voltage. The two profiles represent voltage increase from 0 to 3 V and a decrease from 3 to  $-0.75$  V.

### 5.2.6 Experiments on graphene with an external electric field

To improve upon the results the setup had to be rethought again. The support surface was changed to a glass plate covered with an ultrathin layer of graphene. The graphene cover's flatness was similar to mica's, but it was conductive.

Figures 5.17a and 5.18 shows the samples used for data collection. Two or three areas on each images were chose for analysis. The results of the height change can be seen in figures 5.19-5.21.

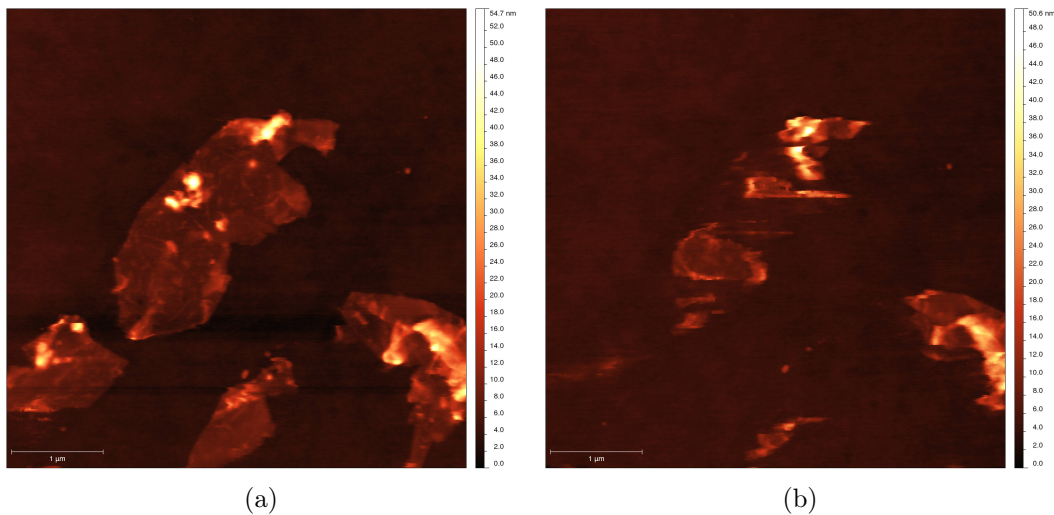
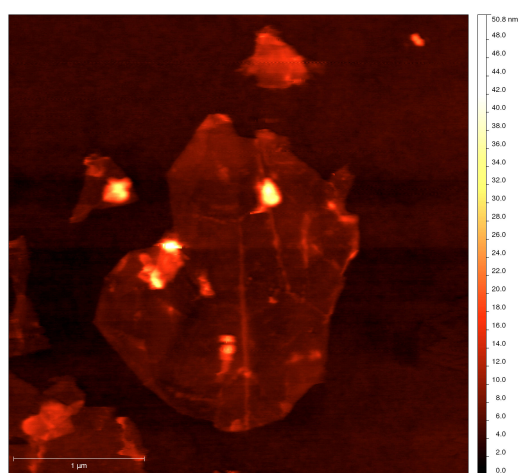
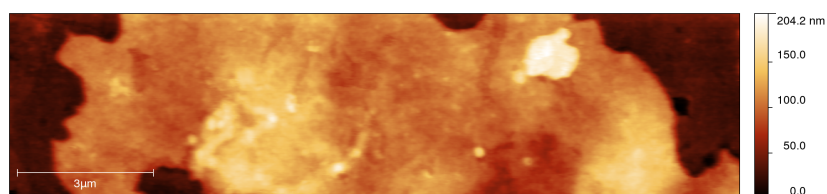


Figure 5.17: First sample on graphene support for data analysis. Image *a* shows how the sample looked during imaging, this particular one was for 0.2 V. Image *b* illustrates how a sample can suddenly be washed away. This happened at 1 V.



(a)



(b)

Figure 5.18: Second (top) and third (bottom) samples on graphene support for data analysis. The areas used on the bottom image are actually to the left and right of the large structure.

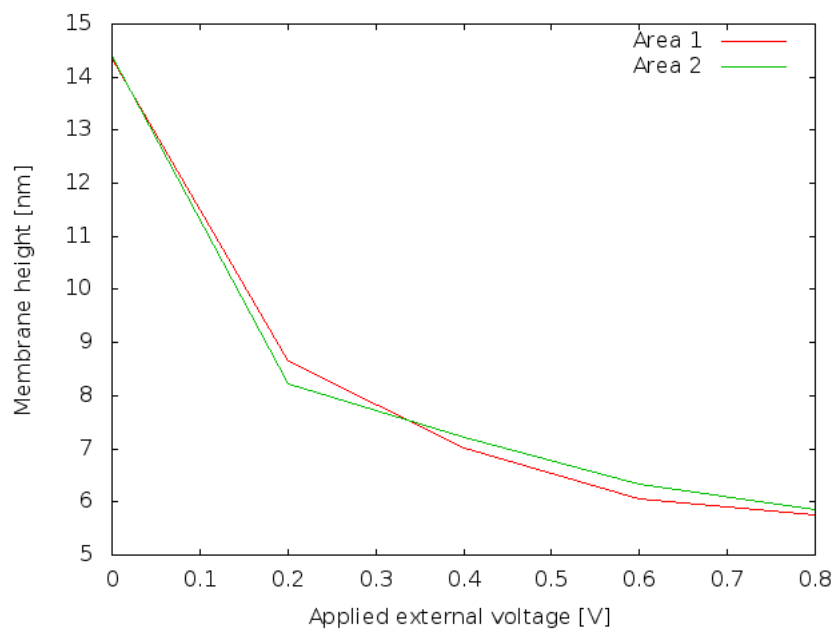


Figure 5.19: Results obtained from image 5.17a on graphene.

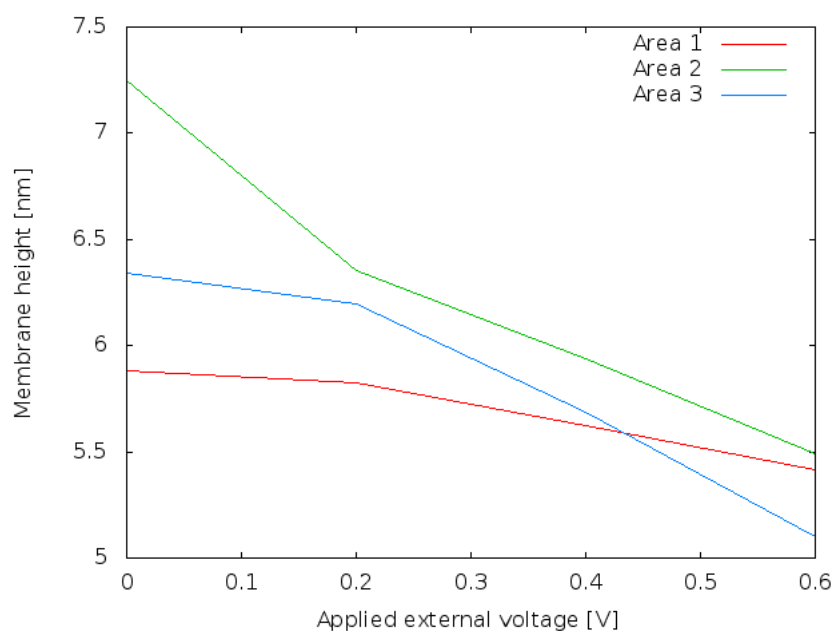


Figure 5.20: Results obtained from image 5.18a on graphene.

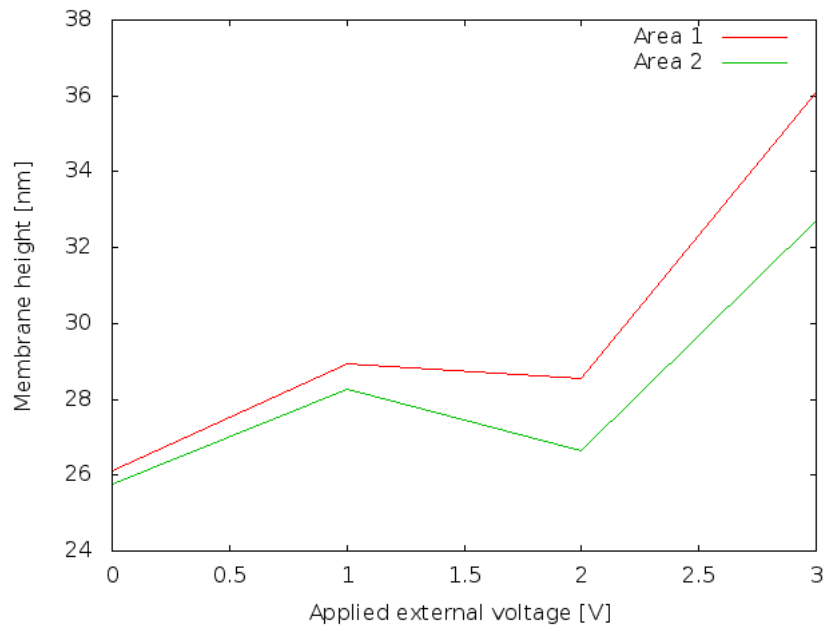


Figure 5.21: Results obtained from image 5.18b on graphene.

# Chapter 6

## Discussion

The results show two effects. One is the decrease in the membrane thickness at lower voltages, the other is the increase in membrane thickness at higher voltages. This is true for experiments both on ITO and graphene as support.

The decrease in the thickness of the lipid bilayer (Fig. 5.15, 5.19, 5.20) is likely related to a state change of the membrane – the voltage increase pushes the membrane through the phase transition, and it goes towards a more fluid state to some extent. Electrostriction could also play a role [38]; the membrane finds itself under the effect of an external electric field that builds up charge on its two sides. This will lead to a compressing force on the membrane, as differently charged ions will attract. The results are only to be taken as a phenomenological proof of theory, because the relation between height and voltage highly depends on the specific experiment.

The high voltage case is different (Fig. 5.16, 5.21), and a rise in membrane height is observed. At this point the membrane is likely completely fluid. These results were observed for several layers of membrane, so an explanation could be an influx of water between the layers, because they would be free to move. Judging from the data in figure 5.21 and assuming 4-6 membrane layers initially, a 2 nm layer of water [37] between each would roughly correspond to the added height. The steps of voltage increase are large in these experiments and overshoot the low-voltage effects seen in the first images; it is therefore possible for such effects to have occurred during these tests as well. To obtain more reliable results with statistical significance, additional experiments have to be made.

The results using graphene covered plates as support were substantially better than the ones obtained on ITO due to the smoothness of the graphene. ITO plates were very rough and had grooves or clefts of the order of a membrane height. It is therefore difficult to say whether they were filled out by lipid material and to what extent. Electric forces and pressure must also have

affected the attachment of the lipids, and the surface could even have acted selectively towards one type of lipid, thereby changing the effective composition of the "free" membrane. In any case the surface distorted the membrane thereby distorting the results as well. It was therefore often difficult to set a zero point in the  $z$ -direction; in figure 5.15 the height of the profile from Image 2 is sometimes below 3 nm, where as expected height for a membrane is about 4 – 6 nm.

A very important point to notice is the return to the initial membrane state after the application of high voltage (Fig. 5.16) on ITO. Due to the fragile state of the membrane, this was difficult to show; indeed in the experiment of figure 5.21, the membrane was destroyed during the increase of voltage to 4 and 5 V. Hysteresis was observed when lowering the voltage.

# Chapter 7

## Conclusion

The main goal of this thesis was to investigate the effect of an external voltage field over a lipid membrane. This was achieved by using a membrane created from the mixture of DPPC and DLPC supported on glass plates covered with indium tin oxide or graphene. An atomic force microscope was used for investigating the thickness of the membrane during the experiments. The following summarises the main conclusions that resulted from these experiments:

- Supported lipid bilayers can be used to investigate the behavior of their phase transition close to room temperature.
- A conductive support material allows for the application of an external electric field over these membranes. It was found out that graphene grown by the CVD method on a glass support creates a good surface for such work due to its flatness.
- Experiments on both ITO and graphene suggested a decrease in membrane thickness and therefore a shift in the phase transition at voltages typically below 1 V.
- Above 1 V the membrane thickness increased. The reason for this is not yet understood, but presumed to be a weaker association between the membrane layers. Thickness change was shown to be reversible but exhibiting hysteresis.
- Interaction with the support material most likely distorted results to some degree. It is known that direct contact with the support can alter the properties of the membrane. An application of hydrogel could be considered to keep the membrane's properties intact.

These results can be used as a basis for future studies on the effect of voltage on membranes. There are several suggestions for improvement on these studies. The use of a hydrogel can be considered to separate the membrane from its supporting material, however, the possible mobility of the membrane should be remembered. Experiments with smaller voltage steps would create a more detailed profile for the decrease in membrane thickness and could also precisely show where and if the opposite occurs. A more systematic approach to voltage application, the time can definitely have an effect. For a simple experiment, a single lipid species could be investigated; having a sharp transition it could be possible to correlate the required voltage to push it through the phase transition as a corresponding change in temperature.

# Appendix A

## Stock solution preparation

This section provides an example for preparing a stock solution. DPPC is used. A 10 mM solution is desired.

- Take the DPPC out from the freezer and let it stand sealed for 15 minutes. Only then open it.
- Measure out approximately 25.5 mg DPPC and add it to a clean flask of 4 ml.
- $\frac{25 \text{ mg}}{734.05 \text{ g/mol}} \approx 34.06 \text{ } \mu\text{mol}$
- $\frac{34.74 \text{ } \mu\text{mol}}{10 \text{ } \mu\text{mol/ml}} = 3.406 \text{ ml}$
- 3.406 ml 2:1 dichloromethane:methanol has to be added to the DPPC powder.
- The solution is then sealed and sonicated slightly. It can then be put in the freezer.



# Appendix B

## Further images

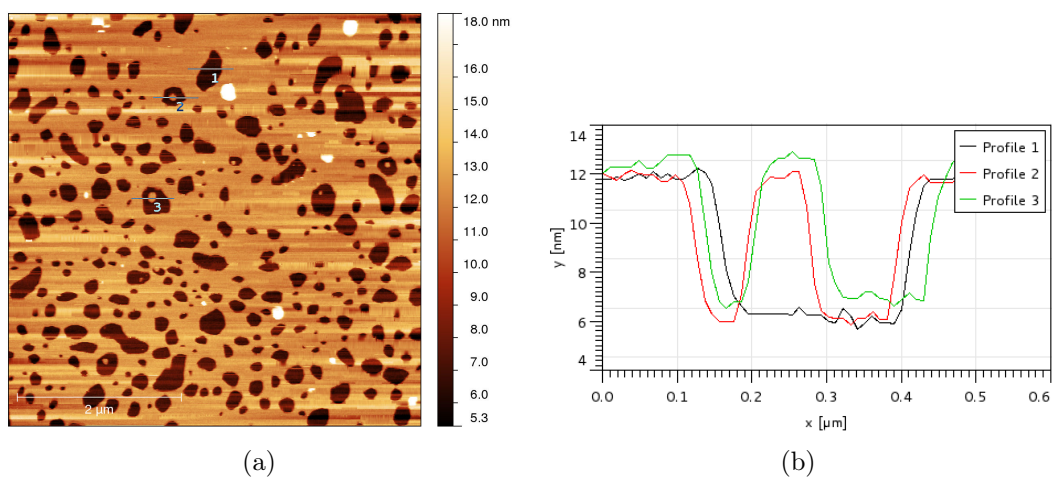


Figure B.1: Pure DPPC on mica in water.

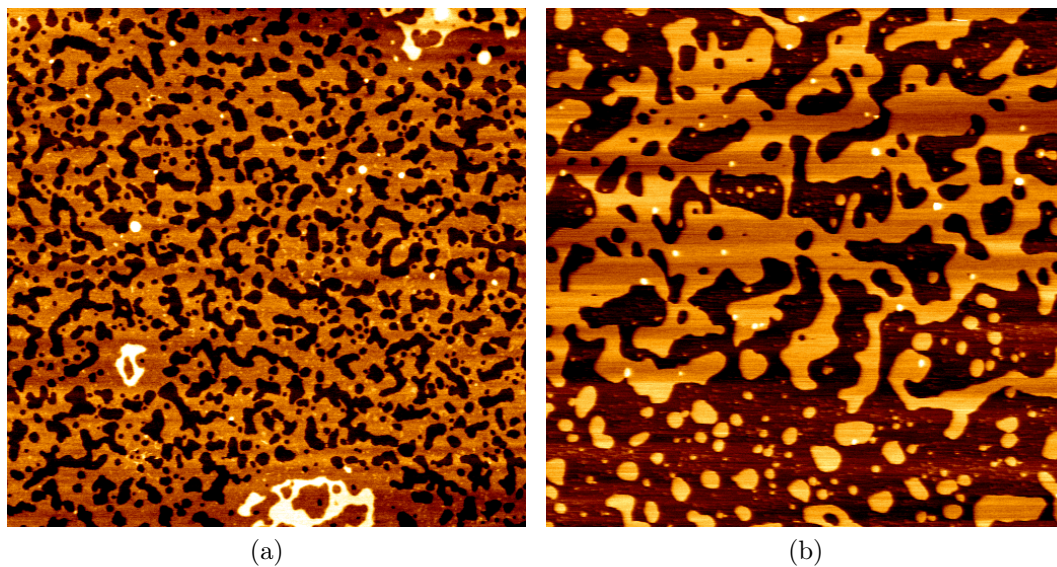


Figure B.2: Additional images of lipid bilayers deposited on mica with clear-cut first, second and third layer.

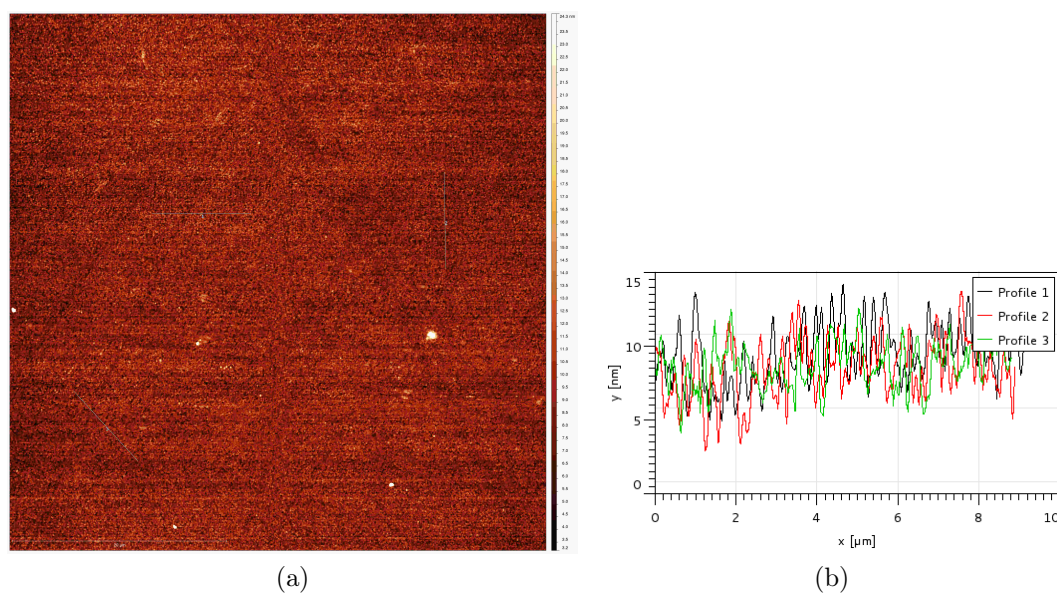


Figure B.3: A very large scan of the ITO background.

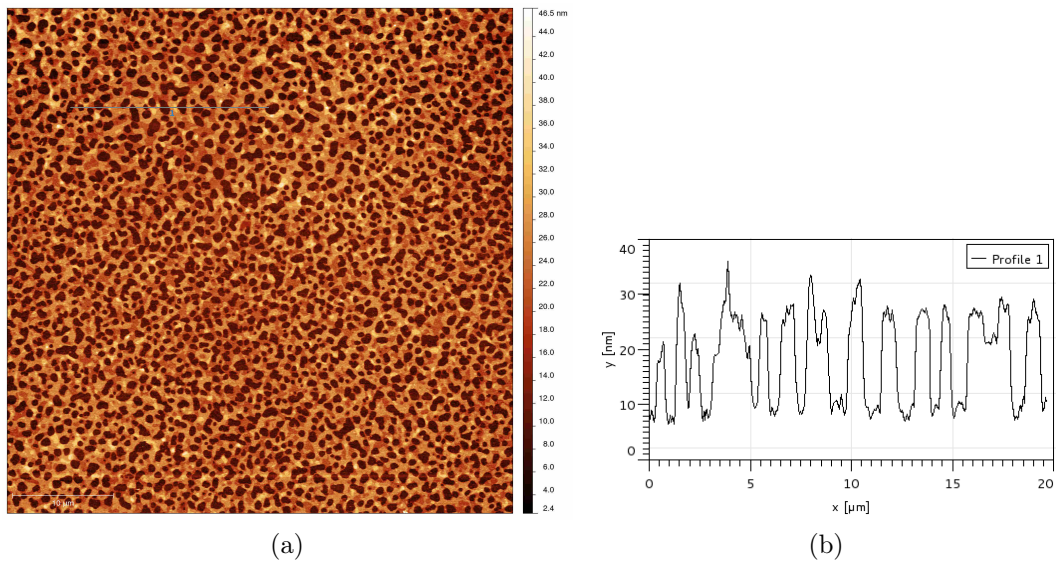


Figure B.4: Figure 5.12 is a zoom in from this picture. It is located in the center, a little to the right and down.



# Bibliography

- [1] A. L. Hodgkin and A. F. Huxley, *Journal of Physiology* (1952).
- [2] T. Heimburg and A. D. Jackson, *PNAS* 102 (2005).
- [3] W. F. P. Pfeffer, *Osmotische Untersuchungen, Studien zur Zellmechanik* (Leipzig, W. Engelmann, 1877).
- [4] E. Gorter and F. Grendel, *The Rockefeller University Press* (1925).
- [5] J. F. Danielli and H. Davson, *Journal of Cellular and Comparative Physiology* (1935).
- [6] A. Blicher, *Electrical aspects of Lipid Membranes*, PhD thesis, Niels Bohr Institute, 2011.
- [7] S. J. Singer and G. L. Nicolson, *Science* (1972).
- [8] O. G. Mouritsen and M. Bloom, *Biophysical journal* (1984).
- [9] E. R. Kandel, J. H. Schwartz, and T. M. Jessell, *Principles of Neural Science*, 4 ed. (McGraw-Hill, 2000).
- [10] H. Jackson, *Thermal Biophysics of Membranes* (Wiley-VCH, 2007).
- [11] <http://avantilipids.com/images/3dc/850355.gif>.
- [12] J. N. Israelachvili, D. J. Mitchell, and B. W. Ninham, *Biophysical Reviews and Letters* (2008).
- [13] L. D. Mosgaard, *Propagation of sound in lipid membranes*, Master's thesis, Niels Bohr Institute, 2011.
- [14] <http://upload.wikimedia.org/>.
- [15] <http://ehumanbiofield.wikispaces.com>.

- [16] Doyle, *Science*, 280 (1998).
- [17] K. Iwasa and I. Tasaki., *Biophysical journal* (1989).
- [18] I. Tasaki, K. Kusano, and P. M. Byrne., *Biochemical and biophysical research communications* (1989).
- [19] J. M. Ritchie and R. D. Keynes., *Quarterly Reviews of Biophysics* (1985).
- [20] B. Lautrup, A. D. Jackson, and T. Heimburg, *ArXiv:physics/0510106v1* (2005).
- [21] B. Lautrup, R. Appali, A. D. Jackson, and T. Heimburg, *The European physical journal* (2011).
- [22] T. Heimburg and A. D. Jackson, *Biophysical Reviews and Letters* (2008).
- [23] H. M. Seeger, M. Fidorra, and T. Heimburg, *Macromol. Symp.* (2005).
- [24] A. M. Baro and R. G. Reifengerger, *Atomic Force Microscopy in Liquid* (Wiley-VCH, 2012).
- [25] G. Schmalz, *Verein Deutscher Ingenieure* (1929).
- [26] H. Becker, O. Bender, and L. Bergmann, *United States Patent Office* (1950).
- [27] R. Young, J. Ward, and F. Scire, *The Review of Scientific Instruments* (1972).
- [28] G. Binnig and H. Rohrer, *Surface Science* (1982).
- [29] G. Binnig, C. F. Quate, and C. Gerber, *Physical Review Letters* (1986).
- [30] P. Eaton and P. West, *Atomic Force Microscopy* (Oxford, 2010).
- [31] C. J. Sullivan, J. L. Morrell, and D. P. Allison, *Ultramicroscopy* (2005).
- [32] <http://prlo.aps.org/>.
- [33] *NanoWizard® AFM Handbook*, , 2.2 ed.
- [34] *JPK NanoWizard® II User Manual*, , 3.3 ed.
- [35] [www.gwyddion.net](http://www.gwyddion.net).

- [36] S. D. Connel and D. A. Smith, *Molecular Membrane Biology* (2006).
- [37] J. Nagle and H. S. Jr., *Biochimica et Biophysica Acta* (1978).
- [38] T. Heimburg, *Biophysical Journal* (2012).